THE FORMATION OF INORGANIC PARTICLES
AT ULTRA-THIN ORGANIC FILMS

By

SCOTT WHIPPS

A THESIS PRESENTED TO THE GRADUATE SCHOOL
OF THE UNIVERSITY OF FLORIDA IN PARTIAL FULFILLMENT
OF THE REQUIREMENTS FOR THE DEGREE OF
DOCTOR OF PHILOSOPHY

UNIVERSITY OF FLORIDA

1996

For Mom

ACKNOWLEDGMENTS

Dr. Augusto Morrone and Eric Lambers at the Major Analytical Instrumentation Center need to be thanked for allowing me to use their TEM and XPS instruments as do Professor Randy Duran and Tim Herod for the use of and help with the BAM experiment.

I'm thankful that my family has always been supportive of me whether or not they understood exactly what I was doing down in Florida. My father, Richard, and brothers Greg, Larry and Ted have shaped me to the person I now am.

Lastly and most importantly, I would like to thank my mother, Cathleen, to whom this dissertation is dedicated. In addition to a million other things to thank her for, she made me believe in myself and realize that any goal is attainable as long as you keep trying.

TABLE OF CONTENTS

THE FORMATION OF INORGANIC PARTICLES AT
ULTRA-THIN ORGANIC FILMS

By

SCOTT WHIPPS

December, 1996

Chairman: Dr. Daniel R. Talham
Major Department: Chemistry

Particles of cadmium iodide were formed at Langmuir-Blodgett films by
reacting the cadmium-containing film with HI gas. In one case a polymerized
diynoic acid film was used as the template for particle growth. The films were
characterized by attenuated total reflectance Fourier-transform infrared
spectroscopy (ATR-FTIR) and ultraviolet-visible spectroscopy (UV-Vis). ATR-
FTIR was also used to follow the reaction that formed cadmium iodide particles.
X-ray photoelectron spectroscopy (XPS) and transmission electron
microscopy/diffraction (TEM/TED) techniques, respectively, identified the
particles as being CdI_2 and determined crystal orientation with respect to the
template. It was found that the polymeric diynoic acid template was able to
guide the formation of many large crystals with the same orientation [(001) face
parallel to film plane] over areas 2.6 μm in diameter. This polymer template did
not, however, appear to limit diffusion of CdI_2 between inorganic layers any

better than a monomeric template. It was suggested that this was due to the template molecule's weak van der Waals forces and the possibility of boundary defects being present around its many small domains.

In a similar study, Langmuir-Blodgett films of octadecylxanthate were also used as a template to grow CdI_2 particles. The xanthate head group was chosen for its potential to interact favorably with iodide layers in the crystal. The xanthate template did exert some control over particles formed, as evidenced by TEM data, where overlapping crystals from different layers in a sample had the same crystallographic orientation over small areas less than 1 μm in diameter. Overall, however, the xanthate template was unsuccessful in controlling crystal orientation. This was due to the template decomposing after the reaction with HI, and giving off CS_2 head groups, as seen by an XPS experiment.

The formation of kidney stones at biological membranes was effectively modeled using monolayers of phospholipids held upon supersaturated solutions of calcium oxalate monohydrate (COM - the main component of kidney stones). Various lipid head groups were studied and it was found that the nucleation process appears to be governed largely by electrostatics. The head groups with more anionic character formed more COM crystals per unit area. In addition, the COM crystal face which nucleated predominantly at the monolayer was the (10$\bar{1}$), a calcium-rich face.

Scope of Dissertation

This dissertation is concerned with the formation of inorganic particles at organic Langmuir-Blodgett films. The focal point of this work has been to study the role of a thin film in directing crystal growth, *i.e.* controlling the crystal's size, shape and orientation. In this way it may be possible to engineer materials at the molecular level, having possible applications in semiconductor as well as optical and magnetic devices, to name a few. Chapter 1 will summarize previous work done in the Talham group on particle formation at Langmuir-Blodgett (LB) film templates as well as provide a literature review on the subject of biomineralization. Chapter 2 describes the formation and characterization of oriented cadmium iodide particles within polymerized diynoic acid LB films. In this project, a polymerized LB film was used in order to limit diffusion of cadmium iodide between layers during particle formation, thereby inducing thinner particles. Chapter 3 is also about CdI_2 particles, but this time they are being formed at an octadecylxanthate LB template. The xanthate head group ($-OCS_2^-$) was chosen for having a potentially favorable interaction with iodide, where the aim was again to make a more 2-dimensional crystal. Chapter 4 describes the nucleation and growth of calcium oxalate monohydrate (COM) crystals underneath floating phospholipid monolayers. Since calcium oxalate is a major component of kidney stones, the lipid systems studied can serve as a

model for kidney stone growth at renal membranes. Various lipids were studied and compared for their ability to form COM. The final chapter presents conclusions and a perspective of the body of work as well as gives possibilities for future work.

Previous Work in the Talham Research Group

Within the Talham group, previous work conducted by Pike investigated the role of an organic Langmuir-Blodgett (LB) film in directing the growth of inorganic particles.[1-3] LB films of cadmium arachidate (Cd-arac) were transferred as Y-type bilayers (where the amphiphiles are aligned hydrophilic head to head, hydrophobic tail to tail, and Cd^{2+} is bound in between layers of anionic head groups, as depicted in Figure 1-1) to a solid support. Upon exposing the LB film to HX gas, where X = I, Br, or Cl, particles of the corresponding CdX_2 are formed within the film. Investigation of the particles was carried out using transmission electron microscopy/diffraction to see how the particles were oriented in the sample, and to learn what effect the LB film had on controlling the particle's size, shape and orientation.

Transmission electron diffraction patterns showed that the CdI_2 particles formed within Cd-arac films were oriented exclusively with their (001) face parallel to the LB film plane. In this orientation, the metal halide layers were parallel to the LB layers. This preferred orientation can be explained by the Cd-arac film's ability to organize Cd^{2+} ions into an arrangement similar to that found in the (001) face of cadmium iodide, resulting in metal halide planes being parallel to LB layers upon crystal growth.
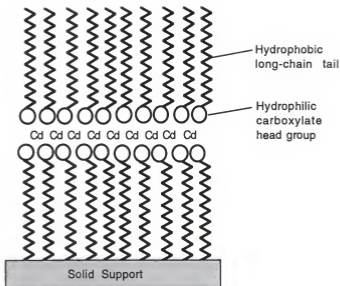
Figure 1-1   Cartoon depiction of a Y-type cadmium arachidate bilayer

When an area of diffraction was used that included many crystals, the diffraction patterns obtained were similar to that of a single crystal, where discrete spots are seen, as opposed to polycrystalline rings. This indicated there were areas of up to 2.6 mm diameter where the in-plane crystal orientations were the same. This uniform in-plane orientation of CdI_2 particles suggested a lattice match between the cadmium iodide and cadmium arachidate LB film. The lattice match may have been responsible for the directed growth of particles. A nearly exact match exists between the Cd-arac LB film and the (001) face of CdI_2, having only a 0.5% lattice mismatch.

In contrast to the CdI_2 system, particles of $CdBr_2$ formed in cadmium arachidate displayed two distinct particle shapes and orientations. One type of particle had a round shape and was oriented with its (001) face parallel to the film, while the other particle type was needle-like in shape and was oriented with the (001) face perpendicular to the LB film plane. The (001) face of $CdBr_2$ has a 7% lattice mismatch with the Cd-arac LB film, which is much larger than that seen in the cadmium iodide system. This may have been the reason for the larger number of allowed orientations in the $CdBr_2$ system. The needle-like $CdBr_2$ particles were found to exist in three preferred orientations that were rotated by 120° with respect to one another. Pike speculated that these orientations could have been a consequence of the in-plane hexagonal close-packing of the LB film.[1]

When Cd-arac films were exposed to HCl to form $CdCl_2$, the resulting particles were also arranged in two distinct orientations, having their (001) faces parallel or perpendicular to the LB film plane as given by their diffraction patterns. This result was similar to that obtained in the $CdBr_2$ system. However, unlike $CdBr_2$, the presence of two types of $CdCl_2$ particles was not detectable from the electron micrographs.

Manganese halide particles were also investigated by reacting the appropriate hydrohalide gas with LB films of manganese arachidate. In general, the MnX_2 particles were smaller than their Cd counterparts. In contrast to the cadmium halides, manganese halides did not produce single crystal diffraction patterns when analyzing many crystals at once. Rather, diffuse rings were obtained. This result indicates that the particles did not share a common in-plane orientation. For all three manganese halide particle systems, it was found that the degree of particle orientation was not as high as that seen in the cadmium halides.

These studies showed that an organized LB film could be used to direct the growth of inorganic particles. In the case of the cadmium halides, the complementarity of the layered CdX_2 structure and the layered LB film may have played a role in orienting the particles. In Chapters 2 and 3, we will explore the effects of changing the organic LB template. A polymerizable diynoic acid template will be investigated in Chapter 2 in order to see the effect a polymerized template has upon particle formation. Chapter 3 will investigate the effects of using a different head group, a xanthate, has upon the formation of inorganic particles.

Biomineralization

Biomineralization refers to the processes by which living organisms form minerals. This phenomenon is widespread, with organisms from all five kingdoms and 55 different phyla forming over 60 known minerals through this process.[4] Approximately half of these minerals contain calcium and most commonly serve as structural support in skeletons or in teeth. The remarkable

control nature exerts over the crystal's size, shape and crystallographic orientation, as well as the properties of the resulting materials such as high strength, resistance to fracture, and esthetic value serve as goals for synthetic materials scientists to reproduce.   Biomimetic chemistry[5] is the field of science that attempts to improve synthetic material design by adapting biological mechanisms that control the formation of minerals at the molecular level.

Nature uses three key points in controlling how inorganic particles are deposited within organic polymer matrices to give organized crystalline arrays.[6] These are ion concentration regulation at the organic matrix/solution interface, growth modification by soluble molecules within the organic matrix, and chemical mediation of crystal nucleation and growth at the organic/inorganic interface by specific interactions at the molecular level.   A transfer of chemical information from the bio-organic matrix to the forming inorganic crystal faces can result in a controlled or regulated crystallization. This allows forming nuclei to be stabilized and crystal growth to be directed.

One of the best understood examples of controlled biomineralization can be seen in the well-studied case of shell formation in molluscs.[7] The mollusc (*Nautilus repertus*) forms its shell of aragonite, a form of $CaCO_3$, upon a thin organic sheet of protein containing acidic polypeptides in the b-pleated sheet conformation. Each $CaCO_3$ crystal is oriented with its *ab* face parallel to the organic sheet. There is a structural correspondence, or epitaxy, between the b-pleated organic layer and the Ca-Ca distances in the *ab* plane of the overlying crystal lattice. Negatively charged aspartic acid residues attached to the b-pleated sheet every 4.96 Å are closely matched with the Ca-Ca distance of 4.7 Å along the a axis of aragonite.[8]   This close geometric correspondence between protein sheet and crystal lattice allows for an organized binding of calcium which lowers the activation energy for nucleation and orients the nuclei

along a preferred direction of growth. Epitaxially controlled crystal growth in organisms, though often suspected, is seldom proven due to the difficulty of characterizing the complex biopolymer matrices where nucleation occurs.

Addadi et al. proposed a model for nucleation and crystal growth for the mollusc shell[9] where sulfate and carboxylate groups on the b-protein sheet act cooperatively in oriented $CaCO_3$ nucleation. In this model, sulfates concentrate calcium ions without permanently binding them to create a localized area of supersaturation. The high concentration of Ca^{2+} is then used by the structured domains of carboxylates (from aspartic acid) to nucleate $CaCO_3$ from its (001) face. The authors created an artificial model substrate of sulfonated polystyrene films absorbed with poly(aspartate). It was found that sulfate-bound substrates did concentrate calcium as seen by ^{45}Ca scintillation counting, and that the combined presence of sulfate and carboxylate groups increased the number of oriented $CaCO_3$ crystals by a factor of three.[9]

Vesicles

In addition to the functionalized protein sheet discussed above, another type of organic assembly that nature employs to control mineral formation is the micellular vesicle.[10] Micellular vesicles, usually composed of lipids, are used by the organism to compartmentalize a small volume prior to biomineralization. The vesicle can maintain the supersaturation, redox and pH gradients necessary to control crystal nucleation and growth. In addition, vesicle size and shape can affect the size and shape of the crystals forming within.

An example of biomineralization within vesicles is demonstrated by magnetotactic bacteria. These aquatic bacteria (several species exist) react to the earth's magnetic field in order to direct themselves toward suitable environments. A row of discrete magnetic crystals made of either magnetite[11]

(Fe_3O_4) or greigite[12] (Fe_3S_4) allows these bacteria to sense changes in the earth's magnetic field. These magnetic particles are single domain, membrane-bound crystals that have uniform shape and a narrow size distribution (50 - 90 nm). The organic membrane that surrounds the crystal plays a central role in the process by providing an enclosed, microscopic regulated area for the crystal formation (a solid state reaction) to occur. Some species of bacteria formed crystals which displayed unique morphologies that could not be reproduced synthetically. This indicated to the authors that some sort of direct biological intervention took place such as the addition of a face specific crystal growth inhibitor.[12]

Phospholipid vesicles lend themselves readily as model systems for biomineralization. By forming the vesicles in a solution containing a species of interest, the species can be encapsulated within the vesicle and is then held captive for subsequent solid state reactions with membrane-permeable species such as OH^- and H_2S. Restricting a chemical reaction to the vesicle interior enables control to be exerted upon supersaturation levels, stereochemical requirements for ion binding and nucleation, and the spatial organization of crystal growth and morphology.

In one study, the effects of vesicular compartmentalization on the reaction of Fe^{3+} and Fe^{2+} with OH^- were investigated.[13] The precipitation of Fe(II) and Fe(III) oxides inside the vesicles was accomplished by raising the pH of the extravesicular solution. This caused OH^- to diffuse into the vessicle where the desired reaction could occur. Iron oxide formed inside the 300 Å diameter phospholipid vesicles of phosphatidylcholine differed in structure, morphology, and size compared to precipitates formed in bulk solution. For example, intravesicular solutions of Fe(II) produced Fe_3O_4 crystals 30-50 Å in diameter upon reaction with hydroxide. In contrast, bulk oxidations produced mixtures of

a- and g-FeOOH. The authors attributed the observed differences between vesicle and bulk reactions to the vesicle membrane's ability to regulate the rate of OH⁻ diffusion into the intravesicular solution, thereby regulating the rate of precipitation. Another difference was that all particles formed within vesicles were either spherical or disk-shaped, whereas bulk precipitates were not rounded. It was presumed by the authors that the initial stages of crystal growth within vesicles were partially constrained by the curvature of the vesicle membrane, resulting in rounded crystal morphologies.[13] The influence of the curved organic substrate in these crystallization reactions is readily apparent. The membrane surface acts as a charged template for ion localization and crystal formation. Also, the hydrophobic membrane acts as a barrier to the external solution, limiting diffusion into the reaction site while the shape and dimensions of the vesicles impart spatial restrictions on crystal development.[10] These factors result in changes of crystal structure, size, and morphology compared to the same reactions carried out in the absence of vesicles.

Surfactant vesicles have been used to produce semiconductor particles of CdS and ZnS.[14] The main point of using vesicles in this work was to limit the size of the particles formed, which have potential use in the areas of molecular electronics and catalysis. Semiconductor particles formed using dihexadecylphosphate measured 2 - 8.5 nm in diameter and were found by electron microscopy to nucleate at the phosphate head groups on the vesicle surface. The authors stated that the discrete nuclei, spatially organized and isolated on the vesicle surface, would not be as likely to aggregate as would be nuclei in free solution, and that this may be why particle sizes were restricted below 10 nm.[14]

One drawback of vesicles is that they are rather delicate and cannot withstand extreme reaction conditions such as high temperature. This is not

surprising for these organic assemblies since weak hydrophobic van der Waals forces are what hold the vesicle together. One study found a more robust alternative to surfactant vesicles in the use of a biological molecule: the cage-shaped iron-storage protein ferritin.[15] Ferritin was used to make nanometer sized FeS particles by reacting the native iron oxide in the ferritin ($5Fe_2O_3 \cdot 9H_2O$) with H_2S gas. Oxides of manganese and uranium were also formed in the ferritin cage once the native iron oxide was removed using dialysis techniques. However, electron diffraction analysis showed these oxides to be amorphous and their identities were not determined.

Langmuir-Blodgett Films

Another route to obtaining an organized assembly of organic molecules which can be used as nucleation sites for studying biomineralization and biomimetic chemistry is the Langmuir-Blodgett (LB) film. LB films serve as a versatile model for biomineralization. In these experiments, a monolayer film of an amphiphilic molecule is compressed and held upon a subphase solution that is supersaturated with the inorganic species of interest. Crystal formation may then occur at the solution/monolayer interface where the surface of hydrophilic headgroups are located. LB films can be tailored in such a way as to help regulate crystal growth in a desired manner. By changing the head group of the LB film, for example, from a sulfate to a carboxylic acid, one can control the chemical nature of the sites where crystal nucleation and growth occur. In addition, by regulating the degree of film compression, one can control the organization and packing of molecules. Most importantly, this allows for control over the spacing of head groups, where ion concentration and nucleation occur.

In one of the early studies of crystallization at LB monolayers, it was determined that structural information could be transferred from the monolayer to the crystals growing underneath[16,17] using a chiral LB system. In this work, Landau *et al.* made monolayer films from chiral a-amino acid amphiphiles that terminated with either R- or S-glycyl head groups. The subphase was a supersaturated solution of racemic glycine. When an R-monolayer was compressed, the head groups simulated an R-layer of a glycine crystal exposed at its (010) face. This R surface gave a stereochemical match for S-glycine molecules to come out of solution and nucleate. Conversely, when using an S-monolayer, the head groups simulate the (0$\bar{1}$0) glycine face and pull R-enantiomers out of solution to form oriented crystals. In each case, structural information from the monolayer was transferred to the crystal in determining which crystal face of glycine formed at the interface. The authors illustrated the importance of head group spacing by varying it through the incorporation of perfluorinated or cholestanoyl moities which decreased and increased head group spacing, respectively. When head group spacing was reduced, some control over orientation was lost, as crystals nucleated at both the (010) and (0$\bar{1}$0) faces for a given enantiomeric monolayer. Increasing the distance between head groups nearly eliminated crystallization at the monolayer/solution interface altogether.[16] In a similar but more thorough study of glycine crystallization under a-amino acids that used grazing angle x-ray diffraction to determine structure of the floating monolayers,[18] Landau *et al.* concluded that the packing of the head groups determines nucleation rates and the degree of orientation of the attached growing crystals.

The Landau group has also investigated the growth of sodium chloride crystals beneath monolayers of long chain carboxylic acids such as stearic and arachidic acid.[17] In these studies the crystal nucleated from a crystal face that

does not occur in nature. However, monolayers were found to stabilize crystal faces that do not occur naturally. The nucleation of NaCl is less specific than glycine since the structure of the monolayer cannot simulate the first layer of the crystal face as seen with the chiral glycine study discussed above. The nucleation of sodium chloride was primarily due to electrostatic interactions between Na+ ions and monolayer head groups. In contrast to bulk solution precipitation of NaCl, where cubic crystals showing their (100) faces result, NaCl grown under monolayers of stearic and arachidic acid gives sodium chloride attached to the monolayer at the (111) face. This face is comprised entirely of sodium ions. By concentrating a layer of sodium ions underneath the layer of negatively charged carboxylate groups, nucleation of the (111) face may be induced.[17]

Mann *et al.* have studied the controlled nucleation and growth of $CaCO_3$ beneath monolayers of stearic acid,[19,20] octadecylamine,[21,22] eicosyl sulfate and eicosyl phosphonate.[23] In these experiments, a LB monolayer was compressed and held upon a supersaturated calcium carbonate subphase solution.

In control experiments, where crystals precipitated in the absence of a monolayer, $CaCO_3$ was in the form of calcite crystals located around the sides and bottom of the LB trough. However, when the supersaturated solution was underneath an organized stearic acid monolayer, the vaterite form of $CaCO_3$ formed exclusively at the monolayer/solution interface, oriented with the (001) faces parallel to the monolayer plane.[19] Compression isotherm data indicated to the authors that Ca^{2+} was incorporating into the head groups of the film to form a layer of calcium which could mimic a crystal face.[20] This electrostatic step alone could not explain the selective formation of vaterite over calcite, since the (001) face of both forms is comprised entirely of Ca^{2+} ions. It was

necessary to investigate the stereochemistry of the forming face. In calcite, the carbonate anions are oriented parallel to the (001) face, whereas in vaterite they are perpendicular. This latter arrangement is equivalent to the orientation of carboxylate head groups in the monolayer. The stereochemical arrangement of carboxylate groups in the LB film mimics the (001) face of vaterite and therefore favors vaterite nucleation over that of calcite.

The observed selectivity with which a preferred crystal face nucleates at the monolayer is related to a stereochemical complementarity between the oxygen atoms of the surfactant's head group and the oxygen atoms of carbonate ions in the nucleating crystal face. Monolayers having sulfate and phosphonate head groups, when compressed on supersaturated calcium bicarbonate solutions, promoted the nucleation of calcite at the (001) face.[23] Electrostatics and symmetry also play key roles in crystal nucleation with the negatively charged sulfate and phosphonate films. The pseudohexagonal close packing of both the sulfate and phosphonate monolayers is similar in symmetry to the hexagonal array of calcium ions in the (001) face of calcite. In this way, calcium bound to the negatively charged monolayers will create a surface of calcium ions which mimics the calcite (001) face.[23]

In contrast to stearic acid monolayers, which produced vaterite nucleated exclusively from the (001) face, nucleation of $CaCO_3$ under a positively charged monolayer of octadecylamine produced vaterite nucleated at both the (001) and (110) faces in equal amounts.[21] Due to the positively charged head group, the binding of Ca^{2+} to the monolayer is not possible. It then follows that a layer of Ca^{2+} that mimics a crystal face could not be formed, as observed with the carboxylate monolayers. The authors speculated that a different mechanism was responsible for the nucleation. Bicarbonate anions from the subphase solution could act as bidentate ligands, binding to the $-NH_3^+$

headgroups. This may provide a stereochemical recognition between carbonates organized within the boundary layer and carbonates in the nucleating faces of vaterite.[22]

The Mann group has also studied the nucleation of $BaSO_4$ underneath monolayers of long chain sulfates,[24] carboxylates [25] and phosphonates.[26] Oriented barium sulfate nucleated underneath eicosylsulfate monolayers exclusively with the (100) face parallel to the monolayer. However, a different crystal face, the (001) face of $BaSO_4$, had a good potential lattice match with a hexagonal array of sulfate headgroups. The fact that the (001) face was not nucleated showed that an epitaxial relationship was not the primary factor in determining crystal orientation. The authors concluded that monolayer-induced oriented nucleation depended on the organic film's ability to mimic both the lattice geometry of cations and the stereochemistry of oxyanions in the nucleating crystal face. At least two recognition processes are in effect at the monolayer/inorganic interface. There is a geometric matching between close-packed head groups and Ba-Ba distances in the crystal lattice as well as a stereochemical complementarity between the sulfate head groups of the monolayer and the sulfate anions of the nucleating crystal face.

Using a technique other than precipitation to grow inorganic particles at an organic template, Langmuir-Blodgett films of arachidic acid have been reported to induce the epitaxial growth of PbS crystals.[27] In these experiments, lead sulfide crystals were formed by forming a LB film of lead arachidate on the trough and then exposing it to H_2S gas. The uniformly sized, equilateral triangle-shaped crystals had their [111] axes perpendicular to the monolayer and their [1$\bar{1}$2], [$\bar{1}$2$\bar{1}$], and [2$\bar{1}\bar{1}$] axes parallel to the monolayer, arranged in 3-fold symmetry at 120° angles. In control experiments where no monolayer was present, only irregularly shaped, non-oriented PbS crystals formed. The growth

of PbS under arachidic acid monolayers was believed to be epitaxial in nature by the authors due to a nearly perfect lattice match between the nucleating (111) face of PbS and the (100) plane of the hexagonally close-packed monolayer.

In Chapter 4, we will use LB films of lipids to model biological membranes for the formation of calcium oxalate monohydrate in experiments similar to those performed by Mann *et al.* described above. This project has potential biological relevance, since calcium oxalate monohydrate is a major component of kidney stones, and its nucleation and growth at lipid monolayers is analogous to stone formation in the kidneys.

FORMATION OF CADMIUM IODIDE PARTICLES AT A POLYMERIZED LANGMUIR-BLODGETT TEMPLATE

Introduction

An objective of this work has been to prepare single layers of an extended inorganic lattice. Once such a system was achieved, it would allow for the study of properties such as magnetism and conductivity within the two-dimensional limit of a monolayer. The strategy used in our group is to take an organic Langmuir-Blodgett film containing metal ions, for example, cadmium arachidate, and react it with a hydrogen halide gas to produce metal halides within the film.[1-3,28] The layered inorganic compound CdI_2 was chosen for study since its layered nature may favor the formation of an extended monolayer over bulk crystals within the LB films. In addition to acting as a template for controlling inorganic crystal growth, it was hoped that the LB film of arachidic acid would act as a barrier against the diffusion of CdI_2 between layers which would lead to bulk particles. It was found that the arachidic acid template was successful in forming CdI_2 particles which were exclusively oriented with their 001 crystal faces parallel to the layer plane. However, this template produced only particles; no evidence for the formaton of an extended inorganic lattice monolayer was observed.[1]

The focus of the current work is to use a LB template that may better limit diffusion between inorganic layers. For this reason a polymerizeable,

diacetylenic acid, 10,12-tricosadiynoic acid, was chosen. This diacetylenic acid has been shown to form a stable film on the Langmuir trough.[29,30] Once polymerized by UV radiation, the resulting close-knit polymer film may effectively prevent or limit the diffusion of CdI_2 between layers when reacting the film with HI gas.

In studies by other groups, polymerized LB films of tricosa-, pentacosa-, and heptacosadiynoic acid have been investigated as photolithographic resists.[31-33] The resist films were evaluated by the resolution obtained (e.g. the minimum distance between two separate photolithographic features) after exposure by excimer laser, x-ray, and electron beam. Ogawa reported that films of pentacosadiynoic acid, which were transferred from Ca^{2+} containing subphases, performed best as resists, having a resolution of 0.3 mm.[32] The authors believed that the resolution was limited by the lens and mask used in the experiments, and, therefore, higher resolutions were possible with the diynoic acid films.

Diynoic acids as well as a few of their derivatives have been investigated for their nonlinear optical properties.[34] In one study,[35] a new optical device was proposed based upon a reversible color change of the polymer film when it is annealed for 10 min. at 60° C. The proposed device could operate as an optical switch. A probe light controls the color phase of the film which in turn determines whether or not the input light is allowed to pass through the film.

The polymerization of 10,12-tricosadiynoic acid from its cadmium salt in monolayer films was first described by Tieke.[36] Exposure to UV radiation results in the formation of a linear, one-dimensional polymer backbone that has conjugated double and triple bonds, as depicted in Figure 2-1. The polymer films have been characterized by infrared spectroscopy and electron diffraction.[30]
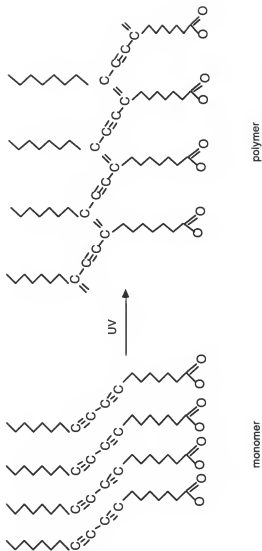
Figure 2-1. Polymerization scheme for a diynoic acid

Diynoic acid films undergo color changes from a colorless monomer to a blue polymer after approximately 30 min. exposure to UV light. Further UV exposure or heating results in a change of color from blue to a bright red color. A phase change in the film from a monoclinic to an orthorhombic arrangement of the alkyl chains is generally accepted as the reason for the thermochromic behavior of the film. Rearrangement of alkyl chains in these films stresses the conjugated polymer backbone and results in a shift of the p and p* electronic energy levels.[37]

An improvement in the layered order of polydiacetylene films was observed upon pre-annealing them before polymerization.[38-41] After annealing for 10 - 20 hr at 42 - 70º C, LB films of 10,12 tricosadiynoic acid (Cd salt) gave more intense x-ray diffraction peaks as well as more orders of diffraction compared to films that were not annealed.[38,39] This indicated to the authors a growth in domain size within the film. In another study on the effects of pre-annealing,[41] polymerized LB films without a pre-anneal step had absorption maxima at 640 nm, while those with a pre-anneal step had their maxima at 704 nm. The authors concluded that the extremely ordered structure of the pre-annealed films (as given by x-ray data) caused the red shift in absorption peaks.

Domain size within the polydiacetylene films is an important issue when trying to form an extended inorganic lattice within them. Large, uniform domains are desirable for this purpose. An electron diffraction study revealed that a polydiacetylene film consists of crystalline domains.[42] Individual domains in adjacent layers were not in registry with one another and the cadmium ions were not located at fixed sites, presumably due to the inclusion of water which partially solvated the Cd^{2+} ions in the interlayer regions.[42] The polymer backbones grew within the layer plane, restricted in their length by the domain size, which averaged from 3 - 100 mm in diameter.[43] Tieke investigated some

factors which affect the domain size. Choice of spreading solvent, subphase temperature, surface pressure of monolayers, the use of mixed monolayers, and annealing all play a role in domain size.[43] Studies were performed using polarizing microscopy. It was found that aromatic spreading solvents increased average domain size by a factor of 10. A subphase temperature of 15 - 20º C, and a surface pressure above 15 mN/m during film transfer also increased domain size. In contrast to results from x-ray studies,[38,39] Tieke reported that annealing the films disordered some molecules and rendered them unpolymerizeable. This led to reduced domain sizes.

Another study[44] used polymerized films of 10,12-nonacosadiynoic acid to grow quantum-state (Q-state) particles of CdS, CdSe, CdTe, and CdS_xSe_{x-1}. The particles were formed by exposing the cadmium-containing film to H_2X gas, where X = S, Se, or Te. Films were analyzed by UV-vis spectroscopy. Neither forming an inorganic monolayer nor controlling particle orientation was the goal of the authors, but it was rather to form particles as small as possible which had shifts in their optical bandgap compared to the bulk materials and posessed non-linear optical properties. The resulting particles ranged in size from 40 - 50 Å. Smaller particle size was obtained by using mixed monolayer films of dihexadecylphosphate and the diynoic acid. The reduction in particle size was attributed to the dihexadecylphosphate causing a reduction in the domain size of the films, where particle nucleation and growth occurs.[44]

In contrast to the previous study, where producing smaller particles is desirable, the work of the current project which will be presented in following sections, aimed to produce large, thin particles approaching monolayer thickness. A cartoon depiction of a cadmium containing diynoic acid bilayer is given in Figure 2-2 as an overview of the steps used to form cadmium iodide particles within the LB film template. Results from this new work show that the
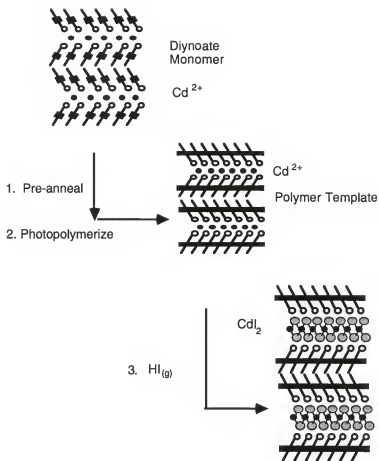
Figure 2-2   Cartoon depicting the formation of cadmium iodide particles at a polymeric template

polymer diynoic acid template produced large CdI_2 crystals that were singly oriented across areas up to 2.6 mm in size. These results are similar to those obtained with the monomeric arachidic acid template.[1,2] The polymeric diynoic acid template was not able to produce a single layer, extended lattice of CdI_2 as desired, at least in part due to the its inability to limit diffusion between inorganic layers. This inability to limit diffusion was attributed to boundaries between domains in the film serving as avenues for metal ions to diffuse between layers, thus forming bulk CdI_2 particles rather than a single layer.

Experimental

Materials

The polymerizeable 10,12-tricosadiynoic acid $(CH_3(CH_2)_9C:::C-C:::C(CH_2)_8COOH$, 98%) was obtained from TCI America (Tokyo, Japan) and stored at $0°$ C away from light until use. Octadecyltrichlorosilane and cadmium chloride hemiheptahydrate $(CdCl_2 \cdot 2.5 \ H_2O$, 98%) were obtained from Aldrich Chemical Company (Milwaukee, WI) and stored under N_2 until use. Hydrogen iodide gas (98%) was purchased from Matheson Gas Products (Atlanta, GA) and used as received. Spectrograde chloroform and hexadecane from Aldrich were used as received. Titanium 300 mesh transmission electron microscope grids were purchased from the Ted Pella Company (Redding, CA) as was the formvar resin used to coat TEM grids. Silicon monoxide (325 mesh powder) was obtained from Aldrich. Single crystal (100) n- and p- type silicon wafers were purchased from the Semiconductor Processing Company (Boston, MA) and were cut into 20 x 15 x 0.5 mm pieces for use as XPS substrates. For all

FTIR measurements, attenuated total reflectance (ATR) silicon crystals, 50 x 10 x 3 mm parallelograms, were purchased from Wilmad Glass Company (Buena, NJ). The water used in LB experiments was purified using a Sybron/Barnstead Nanopure system (Boston, MA) and had an average resistivity of 18 megaohm-cm.

Substrate Preparation

UV-Vis experiments used standard 75 x 25 x 1 mm glass microscope slides that were cleaned using the RCA method.[45] In the RCA procedure, substrates were first immersed in a 5:1:1 by volume mixture of water, 30% hydrogen peroxide, and concentrated ammonium hydroxide for 10 min. at 70° C. Substrates were then immersed in a 6:1:1 mixture of water, 30% hydrogen peroxide, and concentrated HCl for 10 min. at 70° C followed by a thorough rinsing with water. The substrates were then rendered hydrophobic by self-assembling octadecyltrichlorosilane[46] (OTS) as follows. Substrates were immersed in a 2% by volume solution of OTS in hexadecane for 1-3 hr. They were then rinsed for 30 min. with chloroform in a Soxhlett extractor.

The silicon substrates used in FTIR and XPS experiments were first cleaned in a RF plasma etch by placing the substrate in an argon plasma for 15 min. on each side. The substrates were then cleaned following the RCA procecure and made hydrophobic through the self-assembly of OTS as described above.

The substrates used in TEM/TED experiments consisted of TEM grids on top of a microscope slide, covered by about 600 Å of Formvar resin. An electron beam evaporator was used to deposit 300 Å of SiO on top of the Formvar

coated grids, enabling the substrate to then be self-assembled with OTS. In the OTS procedure, hexane was substituted for chloroform in the rinse step.

Instrumentation

LB film deposition was carried out using a KSV Instruments (Stratford, CT) KSV 5000 LB system equipped with a home built double barrier teflon trough. The surface pressure was measured by a platinum Wilhelmy plate suspended from a KSV microbalance.

UV-Vis spectra consisted of 20 scans and were recorded using a Hewlett-Packard 8452A diode array spectrophotometer. Brewster angle microscopy was carried out using a BAM1 Brewster angle microscope by Nanofilm Technology (Gottingen, Germany). The instrument was equipped with a video camera and recorder which allowed for the acquisition of data in real time.

Fourier transform infrared spectra were taken with a Mattson Instruments (Madison, WI) Research Series-1 FTIR spectrometer using a narrow-band mercury cadmium telluride detector. A Harrick (Ossining, NY) TMP stage was used for attenuated total reflectance (ATR) experiments. Spectra consisted of 1000 scans at 2 cm^{-1} resolution and in each case were referenced to the clean OTS-coated silicon ATR crystal.

Transmission electron microscopy/diffraction was carried out on a JEOL (Peabody, MA) JEM 200CX electron microscope. The microscope was operated at an accelerating voltage of 100 kV and beam exposure to the sample was kept to a minimum to avoid sample degradation.

X-ray photoelectron spectra were obtained using a Perkin-Elmer (Eden Prairie, MN) PHI 5000 Series spectrometer. All spectra were taken using the

Mg Ka line source at 1253.6 eV. The spectrometer has a resolution of approximately 1.7 eV, an anode voltage of 15 kV, and a power setting of 300 W. Survey scans were performed at a 70° takeoff angle with respect to the sample surface using a pass energy of 89.45 eV. Multiplex spectra, consisting of 10 scans over each peak, were run over a 30 - 40 eV range with a pass energy of 17.90 eV.

Procedure

Langmuir-Blodgett films were prepared by spreading 100 mL of a 1.0 mg/mL solution of the diynoic acid onto a 4.0×10^{-4} M Cd^{2+} subphase that was cooled to 12° C while at pH 6.2. Approximately 15 mL of a 0.05 M KOH solution was added to the subphase in order to adjust to the desired pH. Subphase pH was again measured at the end of LB experiments to ensure that pH had not changed. Diynoic acid solutions were prepared in the dark in order to avoid polymerization. Chloroform was used as the spreading solvent and films were allowed to spread for 10 min. before compressing. Films were compressed to a target pressure of 25 mN/m at a rate of 5 mN/m/min with maximum barrier speeds of 15 mm/min.

The transfer of LB films to solid supports was accomplished by using dipping speeds of 10 mm/min on the downstroke and 20 mm/min on the upstroke. Samples typcally consisted of one bilayer for XPS work and ten bilayers for TEM experiments. Transfer ratios of the film under these optimum conditions were unity. Before polymerizing the films, the samples were pre-annealed by placing them in a drying oven at 62° C for approximately two hours. This step was done to better preserve the layered structure of the films during polymerization.[38] Photopolymerization of the transferred LB films was

accomplished by placing the sample 20 cm away from a 300 W medium pressure Hg lamp and irradiating the sample for 2.5 hr.

Cadmium iodide particles were then made by exposing the polymerized Cd-diynoate film to hydrogen iodide gas. To accomplish this, samples were held in a 30 mL Schlenk tube fitted at the top with a rubber septum and were evacuated thoroughly before introducing 10 mL of HI gas into the reaction tube using an air-tight syringe. Samples were allowed to react for 5 min. before opening the reaction tube and purging out the HI gas with house nitrogen to stop the reaction. Much care was taken to aviod sample contamination during this procedure.

Results/Discussion

Characterization of Diynoic Acid Template

The material used to form the organic polymer Langmuir-Blodgett (LB) template, 10,12-tricosadiynoic acid, was first characterized in the monomer form at the air-water interface on the LB trough. Monolayers of the diynoic acid collapse at 8 mN/m on a pure water subphase and at 35 mN/m when the subphase is 4.4 x 10^{-4} M CdCl$_2$, as shown in Figure 2-3. The much higher collapse point on the cadmium subphase reflects the strength of the interactions between cadmium ions and carboxylate head groups.

All further studies were carried out on a cadmium subphase since cadmium ions need to be incorporated into the films in order to form cadmium iodide particles. The importance of pH control is illustrated in the
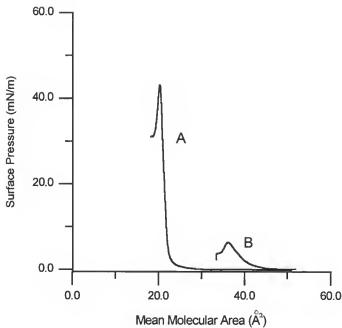
Figure 2-3 Isotherms of 10,12-tricosadiynoic acid on A) 0.44mM Cd(II) subphase and
B) pure water subphase. (Both isotherms at 16 C and pH 5.4)

isotherms given in Figure 2-4. At pH 5.0 the carboxyl groups of the diynoic acid appear to be protonated and cannot interact with metal ions, resulting in the low collapse point. At pH 5.4 the monolayer is much more rigid due to carboxylate/cadmium ion interaction, collapsing at 32 mN/m and having a mean molecular area (Mma) of 23.04 Å^2.

The isotherm at pH 5.4 in Figure 2-4 shows a pronounced transition beginning at a Mma of 33 Å^2. It is suggested that this transition corresponds to the diynoic acid molecule standing to a more upright position from one where part of the molecule (the alkyl chain nearest the carboxyl group) is lying at the air-water interface. Figure 2-5 shows a cartoon depiction of the proposed transition.

A creep test, where barrier movement was monitored while a constant surface pressure was maintained on the film for two hours, was performed on 10,12-tricosadiynoic acid. At the same conditions used for film transfer, the film was very stable, as shown in Figure 2-6, with a creep of only 0.08 mm/min.

Brewster Angle Microscopy

Brewster angle microscopy (BAM) was used to obtain images of the diynoic acid monolayer as it was compressed through its isotherm. The micrograph shown in Figure 2-7 was taken at a surface pressure of 20 mN/m.

The BAM micrograph shows the existence of non-uniform, intricate, feather like structures which appear to consist of many domains. These domains form immediately upon spreading the diynoic acid solution on the subphase and remain even after the film has collapsed. The monolayer existing as many smaller domains rather than one homogeneous domain is an important factor in controlling the formation of CdI_2 particles. This topic will be
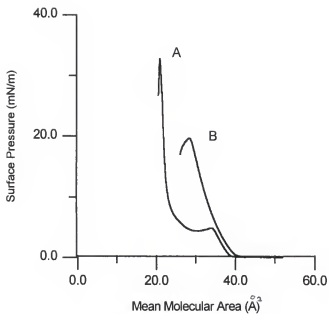
Figure 2-4   Isotherms of diynoic acid at A) pH 5.4 and B) pH 5.0
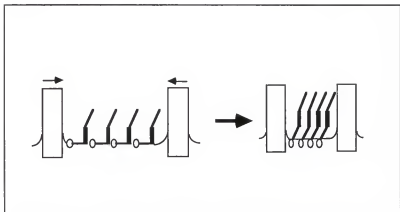(both at room temperature)

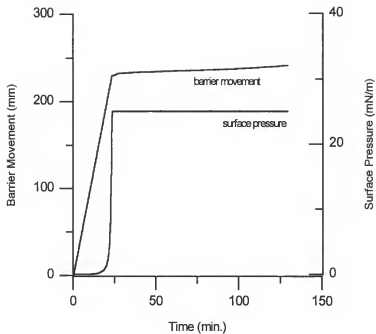Figure 2-5. Cartoon of Proposed Transition

Figure 2-6   Creep test of 10,12-tricosadiynoic acid on a Cd(II) subphase
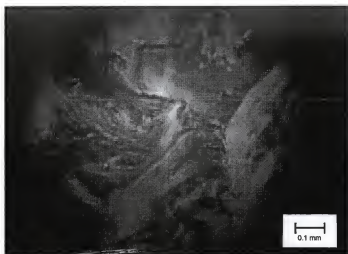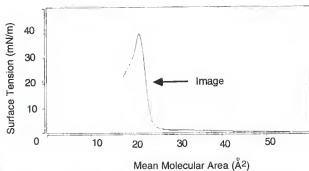
Figure 2-7   Isotherm (top) and Brewster angle micrograph
              (bottom) of cadmium diynoate monolayer taken at a
              surface pressure of 20 mN/m.

discussed in greater detail when the transmission electron microscopy data are presented.

Pre-annealing the samples before polymerization has been shown to increase Bragg peaks in X-ray diffraction studies by as many as seven orders.[40] After annealing, the sample is exposed to UV radiation for 2.5 hr until the polymer is converted to its red form. The sample is then exposed to 5mL of HI gas (at atmospheric pressure) for 5 min., forming cadmium iodide in the inorganic layers and protonating the carboxylate groups of the template.

UV-Vis Spectroscopy

The polymerization of cadmium diynoate multilayers on a glass microscope slide can be followed by UV-vis. To the naked eye, a monolayer of the monomer is colorless, but turns blue after five minutes of exposure to UV light. Further irradiation turns the sample red until no further changes occur after 2.5 hr of exposure. Figure 2-8 follows the photopolymerization of eight bilayers of the monomer through both the blue and red forms of the polymer. Arrows indicate the direction of band growth as polymerization occurs.

Attenuated Total Reflectance IR

Attenuated total reflectance Fourier transform infrared spectroscopy (ATR-FTIR) was used to analyze effects that the pre-anneal and polymerization procedures had upon the organic template as well as to determine the completeness of reaction when forming cadmium iodide. The pre-anneal step had no effect on the IR spectrum of the template. The main effect polymerization
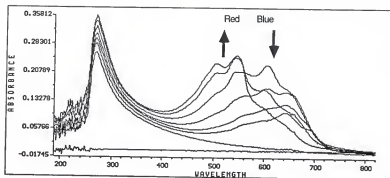
Figure 2-8   UV-vis spectra of 8 Cd-diynoate bilayers after 0, 5, 10, 30, 60, 90, and 120 minutes of exposure to UV light. Arrows indicate direction of band growth.

had on the template IR spectrum was to broaden the asymmetric methylene stretching band at 2921 cm^{-1} (See Figure 2-9). This increase in the full width at half maximum (FWHM) from 26 cm^{-1} in monomer form to 34 cm^{-1} in the polymer indicates that the film becomes more disordered during polymerization. More specifically, the methylene chains of the molecule become less close-packed as the polymerization progresses. Polymerization also resulted in the appearance of a small peak at 1711 cm^{-1} that corresponds to the protonation of some carboxylate groups.

Figure 2-10 is the ATR-FTIR spectra of a polymerized Cd-diynoate multilayer sample before and after exposure to HI gas. The carboxylate band at 1537 cm^{-1} before HI treatment (top spectrum) disappears completely after 5 min. of HI exposure. This information coupled with the resulting carboxylic acid band at 1693 cm^{-1} (bottom spectrum) indicates that all of the template carboxylate groups have been protonated in the reaction to form cadmium iodide particles.

It has been reported that the mode of hydrogen bonding (either facial or lateral, See Figure 2-11) between carboxylic acid groups causes IR shifts in the C=O stretching band.[47] Facial hydrogen bonding between COOH groups gives a band at 1710 cm^{-1} while lateral hydrogen bonding gives its C=O stretch at 1724 cm^{-1}. From the position of the COOH band at 1693 cm^{-1} in the polydiynoic template, it is believed that facial H-bonding is occurring. This is nearly the same peak position seen in the spectrum of neat diynoic acid at 1691 cm^{-1}. By comparison, the carbonyl band of the arachidic acid template [2] had a slightly higher energy at 1701 cm^{-1}, but appears to also form facial H-bonds as in the diynoic template. In order for facial H-bonding in the diynoic template to occur, there can be nothing between the opposing carboxylic acid head groups, as this would interfere with the hydrogen bonding. This indicates that the diynoic
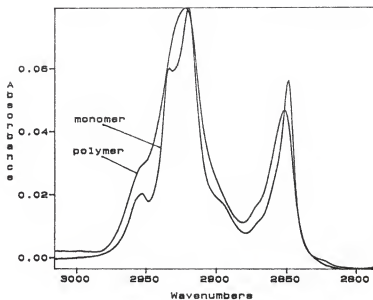
Figure 2-9   The effect of polymerization on the width of the asymmetric methylene band.
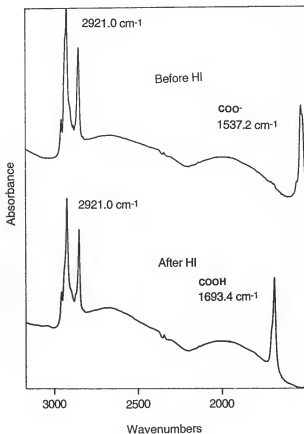
Figure 2-10 ATR-FTIR spectra of a polymerized Cd-diynoate multilayer sample before and after exposure to HI gas.
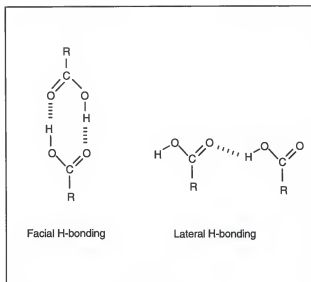
Figure 2-11   Hydrogen bonding modes between carboxylic acid groups

template produced discrete CdI_2 particles (rather than a single layer) and left much of the template's interlayer space empty for facial H-bonding. Had a single layer of CdI_2 been formed, it would have blocked facial H-bonding and only allowed lateral H-bonding, which would have shifted carbonyl bands to higher frequencies.

X-ray Photoelectron Spectroscopy

X-ray photoelectron spectroscopy (XPS), also known as electron spectroscopy for chemical analysis (ESCA), was used to confirm the presence of cadmium iodide formed in samples after exposure to HI gas. A typical multiplex spectrum of a HI treated template is given in Figure 2-12.

The predicted XPS peak intensity ratio for CdI_2 formed in the polymer template was 1.0 cadmium to 1.7 iodide. This ratio was calculated by taking into consideration the effect of photoelectron attenuation by an overlayer and the photoelectron's kinetic energy.[48] An experimental ratio of 1 cadmium to 3 iodide was found in the XPS experiment, which lies outside experimental error of the predicted ratio. The high iodine content cannot be explained by the presence of some excess I_2 formed by the reaction of HI with residual water, because one would expect any I_2 formed to sublime readily under the high vacuum conditions imposed by XPS analysis. A more likely explanation for the higher than expected iodine content is that some of the HI gas is adding onto unsaturated carbon-carbon bonds in the polymer backbone in addition to the expected reaction to form CdI_2 crystals. This line of reasoning will be supported by XPS and TEM data to be presented later. It would not be unreasonable to expect to see some changes in the ATR-FTIR spectra of the polymer template

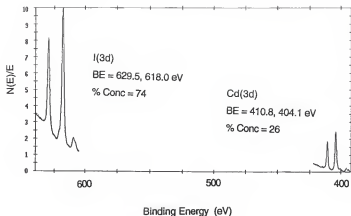Figure 2-12 XPS multiplex spectrum of cadmium iodide formed at the polymer template.

after exposure to HI. For example, the intensity of C-C double and triple bond stretches should decrease after HI adds onto these bonds. However, the intensities of these bands are very weak and they do not lend themselves to quantitation.

When the photopolymerization step was skipped and the template was exposed to HI gas while still in the monomer form, TEM/TED showed no diffraction from CdI_2 crystals (see Figure 2-14). However, when XPS analysis was carried out on an identical sample, a 1 Cd to 4 I ratio was obtained. These results can be explained as follows. When the monomer template is exposed to HI, it reacts both at the unsaturated C-C bonds and at the inorganic layers. However, under the high vacuum conditions used in XPS and TEM/TED, the monomeric template molecules could be volatilized, since weak van der Waals forces are all that hold the monomer template molecules together. Cadmium iodide could have also been removed from the sample by the high vacuum so that no diffraction would be seen in the TEM experiment. However, some monomer template molecules remain on the sample that contain both unreacted Cd^{2+} and iodine that has added onto triple bonds which were detected by XPS in a 1 Cd to 4 I ratio.

When the XPS multiplex peaks for iodine were examined more closely, it was found that the iodine peaks on the polymerized template were symmetrical, while those on the unpolymerized template were asymmetrical, having a slight shoulder at lower binding energy. The shoulder indicates that two types of iodine were present, each with slightly different binding energies as a result of being in different chemical environments. The peaks were analyzed using a peak fitting program, as shown in Figure 2-13. The iodine peaks were fitted using a Gaussian curve that had the same FWHM as in an arachidic acid template sample where the iodine signal is known to be solely from CdI_2. The
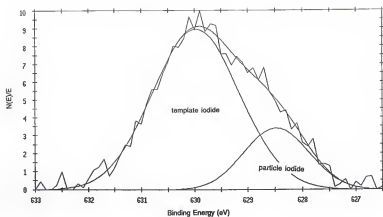
Figure 2-13 Peak fitting of iodine 3d$_3$ XPS peak from a monomer
template.

shoulder iodide peak from the diyne template had the same binding energy as the iodide in the arachidic acid template, indicating that the shoulder iodine peak at 628.4 eV is from iodide in CdI_2 particles. A photoelectron ejected from an iodide ion in the CdI_2 lattice would be expected to have a lower binding energy than the photoelectron ejected from an iodine atom in a covalent environment. This is due to more electron-electron repulsion involved with the anionic iodide than with the covalently bound iodine.

There is a nearly 2 to 1 ratio of covalently bound iodine (major peak) to iodide incorporated into the CdI_2 lattice (shoulder). A possible explanation for this is that the gas appears to react preferentially with the triple bonds rather than with Cd^{2+} when the unpolymerized template is exposed to HI. The absence of diffraction from the monomer template after exposing it to HI is to be expected if the HI is not producing CdI_2, but reacting first with triple bonds.

Transmission Electron Microscopy/Diffraction

Transmission electron microscopy and transmission electron diffraction (TEM and TED) were used to gain structural and orientational information concerning the polymer template and the cadmium iodide particles. When a TEM sample of the polymer template (10 bilayers, no exposure to HI gas) was analyzed it was found not to diffract. Figure 2-14 gives these data.

The domains present in the micrograph of Figure 2-14 are aligned such that the template has a directional grain like appearance. The domains, which form upon spreading the 10,12-tricosadiynoic acid on the water surface, aggregate into superstructures that look like feathers at lower magnification.

Figure 2-14

a)   Transmission electron micrograph of 10 bilayers of polymer
      template before exposure to HI gas.   (Magnification = 10k)

b)   Transmission electron diffraction pattern of 10 bilayers of polymer
      pictured in A) showing no difraction (selected area of diffraction =
      2.6μm).

10 kx

SAD 2.6 µm
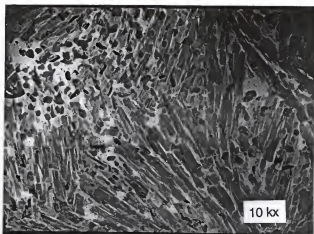
Once the polymer template is exposed to HI gas, the formation of cadmium iodide crystals can be confirmed through its TED pattern. Figure 2-15 shows CdI_2 diffraction patterns as well as the area of the micrograph to which it corresponds. The diffraction pattern in Fig. 2-15 b), taken from the area marked A on the micrograph, shows no diffraction. This region is believed to only consist of the organic polymer since it does not diffract. Note that area A has a different appearance from the polymer template in Figure 2-14 (no HI), with smaller domains separated by very dark regions. The difference in appearance can be explained by the fact that the template in Figure 2-15 could have been chemically altered during exposure to HI, which adds onto unsaturated bonds as discussed earlier.

The next two diffraction patterns, c) and d), in Figure 2-15 are both from the CdI_2 crystal containing area labelled B in the micrograph. In diffraction pattern c), several different orientations of CdI_2 are evident, as given by the presence of diffraction rings rather than discrete spots. For this diffraction pattern a selective aperture of diffraction (SAD) of 2.6 mm was used. However, when the area of diffraction was reduced to 0.7 mm at the same location, only one orientation of CdI_2 was evident. This result is displayed in diffraction pattern d) of Figure 2-15.

Figure 2-16 shows a bright field micrograph of CdI_2 crystals, the diffraction pattern resulting from the entire area pictured (SAD 5.5 mm), and a dark field micrograph of the same area. In the dark field micrograph, the white regions within the dark CdI_2 crystals are most responsible for the (100) diffraction spots. These are the innermost hexagon of the diffraction pattern. Within the entire diffraction area, which measures 5.5 mm across and contains over a dozen cadmium iodide crystals, crystal orientations vary by less than two

Figure 2-15

a)   Transmission electron micrograph of cadmium iodide particles
     (area B) formed at polymer template (area A). (10 bilayers,
     Magnification = 8k)

b)   Transmission electron diffraction pattern taken from polymer area
     A in micrograph above showing no difraction. (SAD =2.6μm)

Figure 2-15 (cont.)

c)   Transmission electron diffraction pattern from CdI_2 particle in area
       B of micrograph. Several crystal orientations are evident using a
       SAD of 2.6 μm.

d)   Transmission electron diffraction pattern of same particle as in c),
       but using a smaller SAD of 0.7 μm. Only one crystal orientation is
       evident.

B - SAD 2.6μm

B - SAD 0.7μm
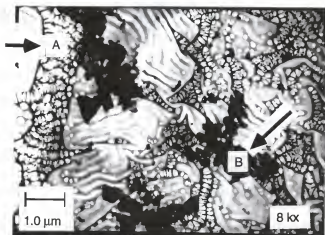
Figure 2-16

a) Bright field micrograph of CdI$_2$ particles formed at a 10 bilayer
polymer template. (Magnification = 10k)

b) Transmission electron diffraction pattern taken from entire area of
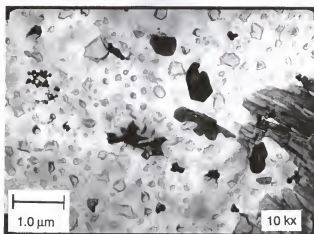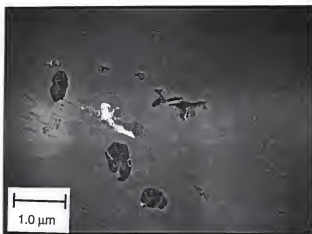micrograph above. (SAD =5.5μm)

1.0 µm   10 kx

SAD 5.5 µm

Figure 2-16

c)   Dark field micrograph of same CdI_2 particles shown in a).
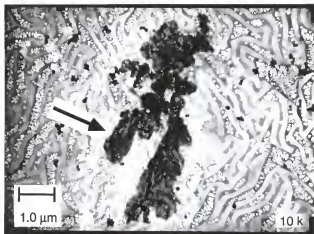(10 bilayers, Magnification = 10k)

1.0 μm

degrees. This is given by the spread of diffraction spots for a given diffraction plane.

Pre-annealing effects are evident by comparing Figures 2-15 (not pre-annealed) and 2-16 (pre-annealed). The pre-anneal step consisted of placing the sample (still in monomer form) in a 62°C drying oven for 3 hr. This procedure did not appear to affect samples as evidenced by a lack of change in the XPS or ATR-FTIR spectra. However, TEM micrographs show that the organic template's appearance was changed by the pre-anneal, taking on a reptilian or alligator skin appearance. In addition to visual differences, the pre-anneal step had the effect of growing a few large CdI_2 crystals (3-5 mm) rather than many smaller ones (< 1mm). This can be interpreted in two ways. First, it is likely that the pre-annealing process allows for the organic template molecules (not yet polymerized) to rearrange into larger domains that allow for larger crystals to form during exposure to HI gas. Or second, the pre-anneal step could make the template contract or could cause defects which would allow for the diffusion of Cd^{2+} between layers, resulting in the formation of large bulk crystals.

Appearances can sometimes be deceiving when analyzing crystals in multilayer samples by TEM. For example, the large CdI_2 structure shown in Figure 2-17 appears to be a single crystal, but its diffraction patterns at several different locations on the structure show that at least two different orientations of CdI_2 are present. Therefore the structure cannot be a single crystal despite its appearance and likely consists of several crystals that are vertically stacked in different layers.

Figure 2-17

a)   Transmission electron micrograph of what appears to be a single
     large CdI$_2$ crystal at the polymer template. (10 bilayers,
     Magnification = 10k)

b)   Transmission electron diffraction pattern taken at area indicated by
     arrow in micrograph above. Pattern shows more than one
     orientation and therefore, did not come from a single crystal.
     (SAD =2.6µm)

Conclusion

The polymeric diynoic acid template was able to effectively guide the formation of large, singly oriented cadmium iodide crystals over areas 2.6 mm in diameter. However, the polymer template did not appear to limit diffusion between inorganic layers significantly better than did the monomer arachidic acid template. This inability to limit diffusion is attributed to the weaker van der Waals forces of the diynoic acid template molecules before polymerization compared to the arachidic acid molecules. The two short C_{10} and C_8 alkyl chains of the diynoic acid molecule do not have as strong of intermolecular forces as does the one long C_{19} chain of arachidic acid. Weaker van der Waals forces allow for many smaller diynoic acid domains to exist compared to the arachidic acid system. If polymerization leaves these smaller diyne domains intact, it may result in the formation of crystals at slightly different in-plane orientations as seen in this work. In addition, defect sites between domains could provide avenues for metal ions to diffuse between layers, forming bulk cadmium iodide particles rather than the desired cadmium iodide monolayers.

CHAPTER 3

FORMATION OF CADMIUM IODIDE PARTICLES AT A LANGMUIR-BLODGETT OCTADECYLXANTHATE TEMPLATE

Introduction

This chapter, as the previous one, is concerned with forming inorganic particles at a pre-formed organic Langmuir-Blodgett film. The LB film may act as a template which directs the formation of these particles, controlling their size, shape and the orientation. The central objective of this project was to form an extended lattice of CdX_2 ($X = Cl$, I) at the template that would have a thickness approaching that of a single layer. This could be thought of as an inorganic crystalline monolayer of CdX_2. In order to achieve this, the interaction between template and the forming crystal must be strong enough to suppress the formation of 3-dimensional structures driven by the crystal's lattice energy. A sufficiently strong interaction between the template and forming crystal would prevent the formation of bulk cadmium iodide crystals in favor of an extended ultrathin inorganic lattice.

Previous work in the Talham group[1-3,28] concerning the growth of oriented inorganic particles at LB templates used a long chain carboxylic acid (arachidic acid, 20 carbons) to construct the organic template. This arachidate template was successful in producing CdI_2 particles oriented exclusively with their layer planes (the 001 faces) parallel to the LB layers. It was believed that

59

the complimentarity in lattices between the layered cadmium iodide structure and the layered LB film was responsible for controlling particle orientation. Though successful in orienting particles, the arachidate template, terminating with its COO^- head group, was not able to produce single layers of the inorganic lattice. Rather, particles with an average size of 0.4 mm were formed.

The approach used in the current project was to change the head group of the LB template to a xanthate, $R-O-CS_2^-$. The terminal atoms are sulfur atoms instead of oxygen atoms in the carboxylate film. The potential advantage of the xanthate head group is to enhance the interaction between it and the 001 surface of CdI_2, which is a surface of iodide ions. Within the cadmium iodide structure, there are two types of bonding interactions present. One is the ionic-covalent bonding between cadmium and iodide ions within the anion-metal-anion layer. These bonding interactions are too strong to be altered by the presence of the LB template. However, the other type of interaction is a much weaker anion-anion interaction between layers in the CdI_2 structure. This weak iodide-iodide interaction is van der Waals in nature. If interactions between the template headgroups and the (001) iodide layer of the crystal can be induced by the proper choice of headgroup, these interactions will compete with iodide-iodide van der Waals interactions of the crystal. In this way, crystals approaching single layer thickness may be favored over bulk crystals.

The sulfur-containing xanthate is a softer, more easily polarizable head group than the oxygen-containing carboxylate. This should lead to a stronger soft/soft interaction of the template head group with the iodide ions of CdI_2, and induce the formation of a thinner oriented crystal.

Compounds having the $-CS_2$ functionality such as xanthates and dithiocarbamates are in general strong chelators and have been used to extract metal ions from mining wastewater. This fact leads one to believe that these

functionalities should be effective in LB experiments, binding metal ions from the subphase. In this work, it is necessary for the hydrophilic head group to bind metal ions from the subphase and incorporate them into the film in order to produce crystals in a later step. Complexes of xanthate and dithiocarbamate compounds have also been used as antioxidants, antiwear lubricants, and vulcanization accelerators.[49]

A limited amount of literature exists pertaining to the use of xanthates or dithiocarbamates in Langmuir-Blodgett experiments. In one study, LB and self-assembled (SA) films of the double chain compound dioctadecyldithiocarbamate were prepared on gold and silver surfaces and compared using IR techniques.[50] It was found that both SA and LB methods produced highly ordered films, but films made by the LB technique had better surface coverage. Also studied was the single chain compound, octadecyldithiocarbamate. This molecule did not form a stable monolayer on the trough and could not be used to produce LB films.

The dioctadecyldithiocarbamate molecule has also been used to make Cu^{2+} containing multilayer samples for an EPR study.[51] It was found that the orientation of the molecules was largely influenced by the dipping direction of monolayers from the water. In another paper[52] the strong affinity of dioctadecyldithiocarbamate for metal ions was utilized to make Cu^{2+} and Ni^{2+} sensors based on the LB technique. The sensor used energy transfer from an underlying fluorescent dye layer to a dioctadecyldithiocarbamate layer with its -CS_2 head groups in contact with a metal containing aqueous phase. Metal complexes formed instantaneously at the LB film/liquid interface and were detected by the presence of their characteristic absorption bands in fluorescence measurements.

It will be shown in the following sections that the goal of forming an inorganic monolayer of CdI_2 inside an LB film template was not achieved using octadecyl xanthate. It was found that crystals from different layers (lying directly above one another) were in registry with one another in some areas less than 1 mm in diameter. However, it was also found that most of the xanthate template decomposed during the reaction with HI during CdI_2 formation. The headgroup, which was hoped to control crystal growth, was given off as CS_2 gas. For this reason the xanthate template failed to control crystal orientation within the layer plane of samples.

Experimental

Materials

Octadecanol (98%) was obtained from Aldrich Chemical Co. (Milwaukee, WI). Analytical reagent grade hexane, ethanol, tetrahydofuran and carbon disulfide were obtained from the Fisher Chemical Company (Pittsburgh, PA). All other materials as well as substrate preparation techniques used were the same as described in Chapter 1.

Instrumentation

All instrumentation used to study the xanthate system was the same as that described in Chapter 1 except for a method used to take transmission IR spectra of xanthate multilayer samples after reacting with HCl gas. A silicon wafer was used as the substrate and was held with the layer planes perpendicular to the incident IR beam. Spectra consisted of 5000 scans at 4

cm^{-1} resolution. A deuterium triglycine sulfate (DTGS) detector was used in order to investigate the S-C band region at 1200 - 800 cm^{-1}.

Procedure

Sodium octadecylxanthate $[CH_3(CH_2)_{17}O\text{-}CS_2^- \text{ } Na^+]$ was synthesized[1] by adding a 10 - 20% excess of CS_2 dropwise via addition funnel to octadecanol and NaOH dissolved in THF while stirring with a magnetic stirrer. The reaction mixture was refluxed for three hours before the yellowish crude product was Soxhlett extracted in hexane for approximately one hour using a cellulose thimble filter. Three recrystallizations gave the product in 80% yield. Identity of the product was confirmed by CHN analysis (experimental : 61.29% C, 10.85% H ; theoretical : 61.96% C, 10.05% H), nmr, and FAB mass spectrometry, where the most intense peak at $m/z = 346$ corresponded to [M - Na]$^+$.

Langmuir-Blodgett films of cadmium octadecylxanthate (Cd-xanthate) were prepared as follows. Chlorobenzene was used as the spreading solvent as this solvent produced a clear solution with the xanthate after heating with a heat gun. Other common spreading solvents did not form a clear solution. Due to chlorobenzene's high rate of thermal expansion, it required great care to ensure the desired amount of material was being spread on the LB trough. The 100 mL of 1 mg/mL octadecylxanthate spreading solution was withdrawn by syringe just as the meniscus of the cooling solution reached the calibration mark of the 10 mL volumetric flask.

The subphase used was 4.0×10^{-4} M CdCl$_2$, chilled to 17° C, and adjusted to pH 6.7 with 0.05 M KOH solution. A delay period of ten minutes passed before compressing the films in order to allow the spreading solvent to evaporate. The xanthate films were compressed at the rate of 5 mN/m/min

using maximum barrier speeds of 10 mm/min until the films reached a target pressure of 30 mN/m. The monolayer was then allowed to sit at the target pressure for 30 min. to allow for the film to stabilize and for the system to reach equilibrium. Dip speeds of 10 mm/min were used on both the downstroke and upstroke to transfer the film to a suitable substrate with transfer ratios of unity. When preparing multilayer samples, care was taken not to completely withdraw the sample from the subphase as not to disturb the monolayer. This technique was found to improve film transfer. One bilayer samples were used for XPS experiments and 8-10 bilayer samples were used for TEM work. All substrates used were made hydrophobic with OTS.

Results/Discussion

Fourier Transform Infrared Spectroscopy

Using the optimum dipping parameters given in the experimental section, the deposition of cadmium octadecylxanthate (Cd-xanthate) bilayers was followed by transmission infrared spectroscopy, as shown in Figure 3-1. The asymmetric methylene band at 2922 cm^{-1} was used to follow the build-up of material. Multiplying the band's intensity by its full width at half maximum (fwhm) gives an estimate of the peak area; this is then plotted as a function of the number of bilayers depositted. The plot is linear through three bilayers, indicating uniform depositions. After four bilayers, however, the peak area deviates negatively from linearity, indicating that less cadmium octadecyl xanthate is being transferred. The lower transfers are believed to be the result
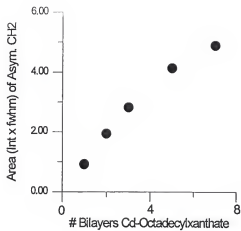
Figure 3-1   Deposition of Cd-octadecylxanthate bilayers followed by ATR-IR

of removing the sample from the LB trough for IR measurements, which tends to disrupt the system. If a sample was dipped continuously without removing, as many bilayers as desired could be transferred with transfer ratios of unity.

The reaction of Cd-xanthate with HCl gas to form $CdCl_2$ particles was followed by IR in order to see the effect HCl gas had on the organic LB film template. Figure 3-2 shows the spectra of 20 bilayers of Cd-xanthate both before and after treating with HCl gas. Overall, the spectrum shows little change after being exposed to HCl for one hour. Of great importance is the preservation of order in the organic template during the formation of inorganic particles. This is desired so that the organic template can play a role in controlling the size and orientation of particles being formed. The position, intensity, and fwhm of the asymmetric methylene stretch at 2922 cm^{-1} indicate that the crystallinity of the alkyl chains is not disturbed by the reaction.

However, the intensities of the asymmetric S-C-S stretching band from the xanthate head group at 1044 cm^{-1} and the asymmetric C-O-C stretching vibration[53] at 1202 cm^{-1} decrease after reacting with HCl. The asymmetric S-C-S band did not shift to higher wavenumbers (as would be expected if protonated), indicating that the reaction did not go to completion. No new peaks appeared in the spectrum after the reaction that corresponded to protonating the xanthate head group. These observations indicated that the template may be unstable. Some of the xanthate head groups may have been lost through decomposition of the LB film, giving off carbon disulfide gas in the process. Further evidence for the decomposition of xanthate will be presented in the XPS data.
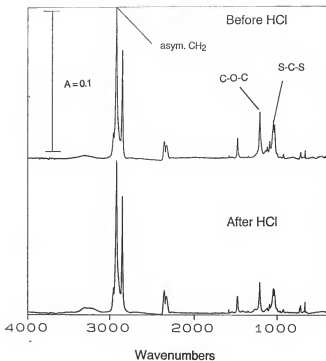
Figure 3-2   ATR-IR spectra of 20 bilayers of Cd-xanthate before and after exposure to HCl gas.

X-ray Photoelectron Spectroscopy

Figure 3-3 contains the XPS multiplex spectrum and relative abundance table for one bilayer of Cd-xanthate that has not been reacted with HI gas. Within this bilayer, an XPS peak intensity ratio of 4.5 sulfur atoms to 1 cadmium ion was predicted. This calculated prediction takes into consideration the effect of photoelectron attenuation by an overlayer and the photoelectron's kinetic energy.[2,48] Experimentally, however, only 2.4 sulfur atoms per cadmium ion were found. The ultra high vacuum conditions (10^{-9} torr) inside the XPS sample chamber caused approximately 47% of the xanthate head groups from the LB template to be given off as CS_2. The xanthate head groups susceptibility to decomposition before reacting to form inorganic particles raised doubt as to its effectiveness as a template.
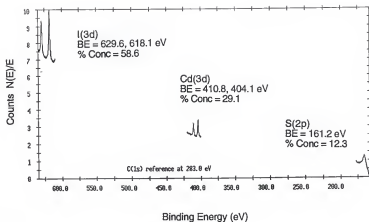
An XPS multiplex spectrum and relative abundance table of the Cd-xanthate bilayer after the reaction with HI to form CdI_2 particles is given in Figure 3-4. The spectrum shows the complete formation of cadmium iodide as expected, with a Cd:I ratio of 1:2. What was not expected was the almost complete absence of sulfur in the spectrum. The sulfur content was less than one tenth of the predicted value. On the average, the sulfur content dropped by 80% in XPS samples after gasing.

The proposed reason for the loss of sulfur in Cd-xanthate samples after reacting with HI is straightforward and is illustrated in Figure 3-5. When HI is introduced to the Cd-xanthate bilayer, the iodide reacts with cadmium to give CdI_2 while the proton bonds to the sulfur of the xanthate headgroup to form a xanthic acid. This xanthic acid is unstable, and readily decomposes[54,55] to give off CS_2 gas, leaving octadecanol behind. These XPS results raised serious
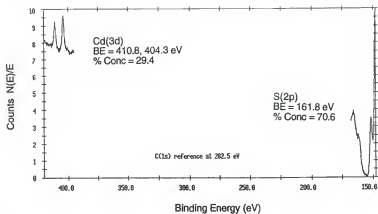
Figure 3-3   XPS multiplex spectrum and relative abundance table for 1 bilayer of Cd-xanthate before exposure to HI gas.

Figure 3-4 XPS multiplex spectrum and relative abundance table for 1 bilayer of Cd-xanthate after exposure to HI gas.
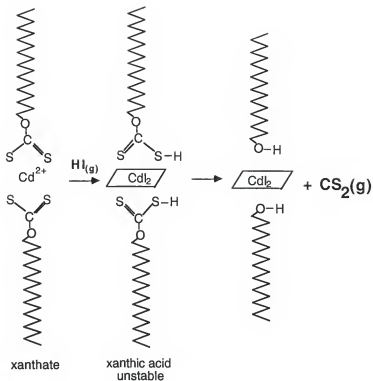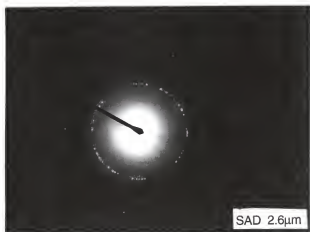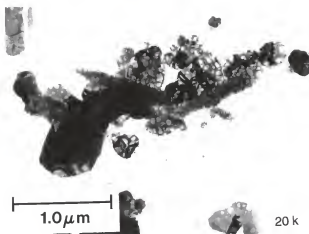
Figure 3-5 The loss of sulfur as seen by XPS after reacting with hydrogen
iodide is attributed to the formation of an unstable xanthic acid,
which decomposes to octadecanol and releases carbon disulfide gas.

doubt as to the effectiveness of the xanthate template. If a considerable amount of xanthate headgroups were leaving during the reaction to form CdI_2 particles, the template would not be effective in controlling particle growth and orientation. Recall that it was the headgroup which was intended to influence the inorganic particle. Once the ramification of these results were realized, further study of the xanthate system was not pursued. It was worthwhile, however, to investigate the cadmium iodide particles that were formed with transmission electron microscopy.

Transmission Electron Microscopy

Figure 3-6 shows a transmission electron micrograph of CdI_2 particles (dark features) formed at the octadecylxanthate template and its corresponding diffraction pattern. These data were representative of the CdI_2 particles formed in the 10 bilayer samples of Cd-xanthate. The micrograph is at a magnification of 20k and the diffraction pattern was taken using a selective aperature diameter of 2.6 mm, which essentially encompasses the entire area seen in the micrograph. The diffraction pattern shows rings rather than discrete diffraction spots as seen in previous work with arachidic acid LB templates. The rings were indexed and found to arise from hk0 diffraction planes. This means that these particles lie with their (001) faces parallel to the layer plane of the sample, as seen with the arachidic acid template. However, the presence of rings rather than spots indicates that the particles do not have the same orientation within the layer plane. The particles are able to exist at many orientations within the layer plane rather than being locked into a single orientation by the template. This lack of control by the xanthate template in limiting the orientation of particles is not surprising when one considers that the xanthic acid head groups

Figure 3-6

a)   Transmission electron micrograph of CdI$_2$ particles formed at an 8 bilayer xanthate template. (Magnification = 20 k)

b)   Transmission electron diffraction pattern taken from micrograph above. Polycrystalline rings indicate particles do not have same in-plane orientation. (SAD = 2.6 µm)

1.0 μm

20 k

SAD 2.6μm

are unstable and are given off as CS_2 gas as evidenced by XPS data. With fewer template headgroups present to interact with forming particles, the CdI_2 would be able to adopt many more in-plane orientations which would give rise to the observed diffraction rings.
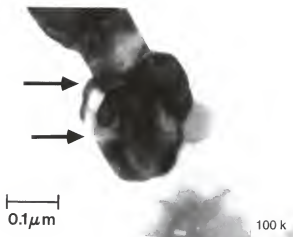
Although octadecylxanthine in general was not successful as a template, due to the instability of xanthic acid and its inability to control inorganic particle orientation, there was one piece of evidence that showed that the xanthate template did exert some control over CdI_2 particles formed. The TEM micrograph in Figure 3-7, taken at a magnification of 100 k, has checkered or fringed areas (indicated by arrows) which are known as Moire patterns. A Moire pattern arises in electron microscope images when the electron beam is diffracted by two overlapping crystals that have equal lattice patterns.[56] In this case, the Moire pattern is due to two overlapping CdI_2 crystals from different layers within the sample. Despite the fact that we are looking at two separate crystals as given by the Moire pattern, the diffraction pattern from this area is that of a single crystal, having cadmium iodide's characteristic hexagonal pattern and showing only one orientation. From the diffraction pattern, it is evident that the overlapping crystals from different layers have the same in-plane orientation, possibly due to the effect of the xanthate template over the 0.7 mm diameter area.

Conclusion

In working with Langmuir-Blodgett films of cadmium octadecylxanthate, it was found that the well ordered system could be used to form CdI_2 crystals with their 001 faces oriented exclusively parallel to the LB layer planes. This aspect

Figure 3-7

a) Transmission electron micrograph of CdI$_2$ particles formed at an 8
    bilayer xanthate template.   Arrows indicate presence of Moire
    patterns. (Magnification = 100 k)

b) Transmission electron diffraction pattern taken from micrograph
    above.   (SAD = 0.7 μm)

0.1 μm

100 k

SAD 0.7 μm

was similar to results obtained using arachidic acid films. Within the layer plane, however, crystals in the xanthate template do not have similar orientations. This was in contrast to the control arachidic acid films have over in-plane crystal orientation of cadmium halides. The reason for the xanthate template's lack of control over in-plane orientation is that the xanthate gave off its CS_2 head group during the reaction with HI gas. Once this occurred, the organic film lost its ability to control the in-plane orientation of the particle as seen in electron diffracton data.

It was hoped that the soft/soft interaction between sulfur atoms of the template and iodide ions of the CdI_2 would overcome the lattice energy that leads to the formation of bulk CdI_2 crystals. However, the interactions between template and inorganic lattice were not achieved due to the decomposition of the template during the reaction to form CdI_2. Although overall the octadecylxanthate template was unsuccessful in controlling the orientation of inorganic particles, there was evidence that overlapping crystals from different layers in a sample were in registry with one another for small areas of less than 1 mm diameter.

CHAPTER 4

USING LANGMUIR-BLODGETT FILMS OF LIPIDS TO MODEL KIDNEY STONE FORMATION AT BIOLOGICAL MEMBRANES

Introduction

Kidney stone disease continues to be a significant health problem that, although treatable through surgery, as yet has no cure. In recent years, one percent of all hospital admissions in the United States were due to kidney stone disease.[57] Calcium oxalate monohydrate, $Ca(C_2O_4) \cdot H_2O$ is the major component in 60 - 80% of kidney stones[58,59] and from this point on will be referred to by its abbreviation, COM.

An objective of the work to be presented here is to show how LB films of lipids can be used as an effective model system for the formation of kidney stones at biological membranes. Information gained on the nucleation and growth mechanisms of COM from an *in vitro* model may give insight on how to prevent kidney stone formation. Figure 4-1 shows cartoon depictions of both a biological membrane and COM crystals forming under a lipid LB monolayer. This figure uses "ball and stick" notation, where the hydrophilic head groups are represented by balls and the lines are hydrophobic aliphatic chains. Some important differences exist between the biological membrane and the LB model. The biological membrane is much more complex, being composed of a mixture of lipids with different head groups, as well as having various proteins
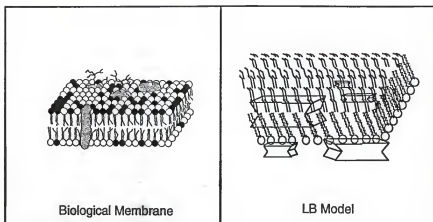
Figure 4-1. Membrane Modeling

incorporated into the bilayer structure. The LB model consists of a monolayer of a single lipid, floating on a supersaturated COM solution, where the level of supersaturation is defined as the ratio of the activity of the experimental COM solution to the activity of a saturated COM solution.[60]

The Langmuir-Blodgett (LB) technique is used to form well-ordered monolayer and multilayer assemblies of amphiphilic molecules and is described elsewhere in greater detail.[61-65] An advantage of the LB technique is the ability to have control over the organization of a film at the molecular level. Langmuir-Blodgett films have been used by Landau et al. in one of the early studies of crystallization at monolayers.[16,17] Here it was determined that structural information could be transferred from the monolayer to the crystals growing underneath. This group has also investigated the growth of sodium chloride crystals beneath monolayers of long chain carboxylic acids such as stearic and arachidic acid.[17] The monolayers were found to nucleate and stabilize the (111) face of NaCl, a face that does not occur naturally.

Mann et al. have studied the controlled nucleation and growth of $CaCO_3$ beneath LB monolayers of stearic acid,[19,20] octadecylamine, [21,22] eicosyl sulfate and eicosyl phosphonate.[23] In these experiments, the monolayer was compressed and held upon a supersaturated calcium carbonate subphase solution. In control experiments, where crystals precipitated in the absence of a monolayer, the calcite form of $CaCO_3$ was formed around the sides and bottom of the LB trough. However, in the presence of a stearic acid monolayer, a different form of $CaCO_3$, vaterite, formed exclusively at the monolayer/solution interface, oriented with the (001) faces parallel to the monolayer plane.[19] Compression isotherm data indicated to the authors that Ca^{2+} was incorporating into the head groups of the film to form a layer of calcium ions.

The calcium ions in this layer could then mimic the calcium positions found in a specific crystal face of vaterite and proceed to grow from this nucleated face.[20]

The Mann group has also studied the nucleation of $BaSO_4$ underneath monolayers of long chain sulfates,[24] carboxylates[25] and phosphonates.[26] The authors concluded that monolayer-induced oriented nucleation depended on the organic film's ability to mimic both the lattice geometry of cations and the stereochemistry of oxyanions in the nucleating crystal face. At least two recognition processes are in effect at the monolayer/inorganic interface. There is a geometric matching between close-packed head groups and Ba-Ba distances in the crystal lattice as well as a stereochemical complementarity between the sulfate head groups of the monolayer and the sulfate anions of the nucleating crystal face.

We are interested in studying the role that the lipid plays in crystal formation. More specifically, we want to determine the effect that varying the chemical nature of the lipid has on crystal formation in terms of the amount, size, shape, and orientation of COM crystals.

Figure 4-2 shows the structures of lipids used in this study. The phospholipids dipalmitoylphosphatidylglycerol, dipalmitoylphosphatidylserine, and dipalmitoyl-phosphatidylcholine vary only in their head group structure. The lipid head groups are believed to be an important factor since they form the surface where nucleation occurs. The COM formation experiments were performed at pH 7.0, at which the lipids in Figure 4-2 are known to exist in the fully ionized state.[66]
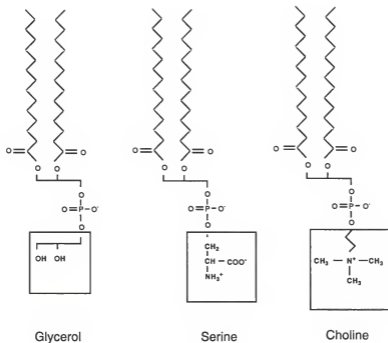
Figure 4-2. Structures of the lipids used to study COM formation:
dipalmitoylphosphatidylglycerol, dipalmitoylphosphatidylserine,
and dipalmitoylphosphatidylcholine.

Experimental

Materials

Dipalmitoyl-L-a-phosphatidyl-DL-glycerol (99%), dipalmitoyl-DL-a-phosphatidyl-L-serine (98%), and dipalmitoyl-L-a-phosphatidylcholine (99%) were purchased from Sigma (St. Louis, MO) and used as received without further purification. Calcium chloride (97%), sodium oxalate (99.99+%), tris(hydroxymethyl)aminomethane hydrochloride (99+%), from Aldrich (Milwaukee, WI) and sodium chloride (99+%) from Fisher (Pittsburgh, PA) were used as received. The water used in LB experiments was purified via a Sybron/Barnstead Nanopure system (Boston, MA) and had a resistivity of 18 MΩ-cm.

Instrumentation

Langmuir-Blodgett experiments were carried out on a custom made teflon double barrier trough measuring 12 x 60 cm and controlled with a KSV Instruments Model 5000 LB system (Stratford, CT). Surface pressure was measured with a platinum Wilhelmy plate suspended from a KSV microbalance.

IR spectra were recorded with a Mattson Instruments Research Series-1 FTIR spectrometer (Madison, WI) using a narrow-band mercury cadmium telluride detector and a Harrick TMP stage (Ossining, NY) for ATR experiments. Spectra consisted of 1000 scans at 2 cm^{-1} resolution and were ratioed to bare ATR crystal background spectra.

TEM/TED analyses were conducted on a JEOL JEM 200CX electron microscope (Peabody, MA), operated at an accelerating voltage of 100 kV. Scanning electron microscopy experiments were done on a JEOL 35C microscope (Peabody, MA) at an accelerating voltage of 15 kV.

A Nanofilm Technology Brewster angle microscope 1 (Gottingen, Germany) equipped with a CCD camera and video cassette recorder was used to observe the surface during compression isotherms and the formation of COM crystals at the monolayer/subphase interface.

Substrate Preparation

Silicon ATR crystals from Wilmad Glass Co. (Buena, NJ) were cleaned and made hydrophilic using a piranha etch (one hour immersion in freshly prepared 3:1 $H_2SO_4 : H_2O_2$) and the RCA cleaning method (ten minute immersion in 70°C solution of 5:1:1 H_2O: H_2O_2: NH_4OH followed by a ten minute immersion in 70°C solution of 6:1:1 H_2O: H_2O_2: HCl and a thorough water rinse.) Glass microscope coverslips used as substrates for SEM analyses were cleaned using a piranha etch. Titanium and copper grids (300 mesh) from the Ted Pella Co. (Redding, CA) used for TEM/TED analysis were mounted onto microscope slides for support, covered with an approximately 600 μm thick film of Formvar resin (Ted Pella Co.) and made hydrophilic by immersion in a 1% (w/v) aqueous poly-L-lysine solution from Fisher.

Methods

Typical parameters used in LB experiments such as isotherms and SEM sample preparation include linear compression rates of 5 mN/m/min, barrier

speeds of 10 mm/min, and target pressures of 20 mN/m. All lipids were dissolved in a 5:1 chloroform: methanol spreading solvent, at concentrations near 1.0 mg/mL.

Supersaturated calcium oxalate monohydrate subphases were prepared as follows. An aqueous solution that was 150 mM NaCl and 5mM Tris HCl buffer was adjusted to pH 7.0 by adding the appropriate volume of 0.05 M KOH (aq). This solution was split into two equal volumes before adding the appropriate amounts of $CaCl_2$ to one and $Na_2C_2O_2$ to the other. This was done in order to avoid precipitation of COM. After these solutions completely dissolved and just prior to their use, they were combined and filtered (≤ 1 μm pore size) to give a final solution that was either 0.35 or 0.5 mM in COM. These subphase solutions had relative supersaturation levels (RS) of 5 and 10, respectively. The computer program EQUIL v.1.3, was used for the calculation of relative supersaturation levels.

The transfer of lipid monolayers to a solid support for analyses by SEM and TEM/TED was accomplished by carefully draining the subphase from the trough, which effectively lowered the monolayer onto a substrate that had been placed in the subphase before the monolayer was applied. Substrates were positioned at an angle of approximately 15° with respect to the bottom of the trough to allow for better drainage. The Langmuir-Blodgett technique was used for monolayer transfer to ATR crystals, using dipping speeds of 10 mm/min.

Results/Discussion

Monolayer Studies

Pressure-area isotherms were obtained for dipalmitoylphosphatidyl-glycerol, dipalmitoylphosphatidylserine, and dipalmitoylphosphatidylcholine repeating the same experimental conditions as previous authors.[67,68] The isotherms obtained were consistent with those previously published. Hereafter, the lipids will be referred to by their head groups: glycerol, serine, and choline. The lipids were also studied by performing creep tests on the supersaturated COM subphase used to grow crystals. All lipid monolayers were found to be very stable on COM subphases, with no loss of film after several hours of holding a constant surface pressure of 20 mN/m.

Pressure-area isotherms of glycerol in Figure 4-3 show a dependence upon subphase calcium concentration. In the range of 6×10^{-6} M to 6×10^{-3} M Ca^{2+} studied, the smallest mean molecular areas (Mma's) were obtained for middle concentrations, while larger Mma's were observed for both the higher and lower calcium concentrations. This result is attributed to an optimum concentration of calcium in the range of 6×10^{-5} to 6×10^{-4} M which binds the monolayer together most effectively. At lower concentrations the monolayer is expanded due to less calcium binding, while at higher $[Ca^{2+}]$ an excess of calcium incorporated into the film caused the expansion.

In the complete absence of Ca^{2+}, lipid monolayers showed higher surface pressures at large (>60 Å^2) Mma's. The addition of a very small amount of Ca^{2+} lowered the surface pressure, due to the Ca^{2+} ion organizing
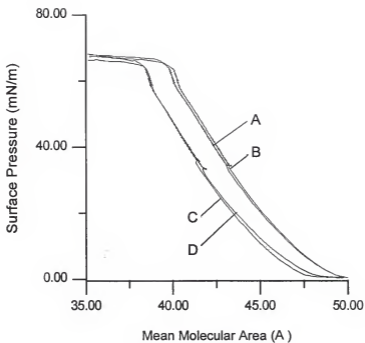
Figure 4-3. Isotherms of dipalmitoylphosphatidylglycerol over varying
subphase calcium concentrations. A) 6 mM; B) 0.006 mM;
C) 0.06 mM; D) 0.6 mM.

the lipid film into more compact domains. The interactions of phospholipids with calcium ions is well documented in the literature.[69-75]

Blank Studies

Blank experiments were conducted where a supersaturated COM subphase at a relative supersaturation level of 10 was allowed to sit in the LB trough without the presence of a lipid monolayer. After periods of up to 21 hr, prepositioned substrates did not have any COM crystals on them as seen by SEM. The remaining subphase was then passed through filter paper with pore size ≤ 0.2 mm. The filter paper was inspected by SEM, and in each case, no COM crystals were observed.

ATR-IR Experiments

ATR-IR experiments of lipid monolayers[76,77] showed the lipid film to be well-ordered and gave evidence of COM formation. Figure 4-4 is the ATR-IR spectrum of a glycerol monolayer after it had been on a supersaturated COM subphase for 21 hr. The broad band at 3300 cm^{-1} is from the hydroxy groups of the glycerol head group. Another band assigned to the lipid is the asymmetric methylene stretch, whose position (2918 cm^{-1}) and shape (FWHM = 19 cm^{-1}) are consistent with a well-ordered, closely packed film, with its alkyl chains in an all trans conformation.[62]

Evidence of COM formation is seen by the presence of the $\partial(\text{HOH})$ water deformation band of COM at 1655 cm^{-1} and a non-fundamental COM vibration

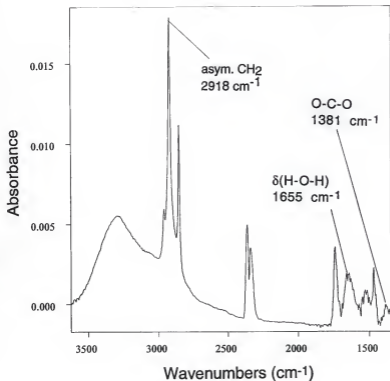Figure 4-4.   ATR-FTIR spectrum of a glycerol monolayer after floating on a supersaturated COM subphase for 21 hours. Bands at 1381 and 1656 cm^{-1} are attributed to COM and give evidence for COM crystal formation.

at 1381 cm⁻¹. The band at 1381 cm⁻¹ is a combination of O-C-O and C-C vibration modes of the oxalate anion. [78,79] The COM bands did not lend themselves for quantitation for two reasons. First, the bands were of very low intensity. Second, the bands were not seen to increase regularly with time as would be expected if the COM crystals were increasing in size or number. This was due to crystals being unevenly distributed beneath the monolayer. In this way, a sample of monolayer taken after four hours of crystal growth may have more COM present than one taken after ten hours.

The IR spectra did show that COM was being formed, but it did not tell if the COM was being formed at the lipid/solution interface or simply precipitating out of bulk solution. To investigate this it was necessary to use Brewster angle microscopy.

Brewster Angle Microscopy (BAM)

BAM experiments showed conclusively that COM was forming at the lipid/solution interface rather than simply precipitating out of bulk solution. In the BAM experiment, polarized light from a He-Ne laser is directed toward a floating monolayer at the Brewster angle (53º for water), the angle at which the intensity of reflected light is at a minimum. This reflected light is then recorded on a CCD camera through a microscope and stored on videotape by a VCR. The Brewster angle microscope sees only what is taking place at the interface, by measuring differences in refractive indices at the monolayer/water interface.

Figure 4-5 is a BAM image of a glycerol monolayer early in a compression isotherm, before surface pressure begins to increase. Individual flower-shaped domains, similar to those observed by Losche et al., [80] using fluorescence microscopy, are apparent before they are compressed together to

Figure 4-5   Brewster angle micrograph of glycerol lipid domains at low surface
              pressure. Image dimensions are approximately 2mm x 2 mm.

93
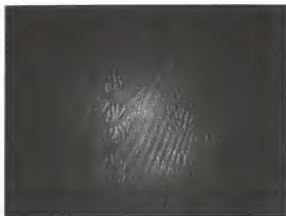
form a homogeneous looking monolayer. The BAM images presented here show sections of the monolayer that are approximately 2 x 2 mm in size. Figure 4-6 is another BAM image of the same monolayer taken after holding surface pressure constant for 90 min. The bright spots are due to birefringent COM crystals. Birefringence stems from the interaction of polarized light with the anisotropic COM crystal lattice. Similar results were seen using serine and choline lipid monolayers. In general, the first crystals are observed within 10 min. after the lipid monolayer reaches its target pressure of 20 mN/m. The results from blank experiments coupled with the fact that crystals are visible using BAM indicate that the crystals nucleate and grow exclusively at the lipid/water interface.

Figure 4-7 is a BAM image of a line of COM crystals grown under a glycerol monolayer. Linear arrangements of crystals were fairly common, especially with serine monolayers. One theory of kidney stone formation states that stones grow preferentially at areas within the kidney where damage has ocurred to remove the protective layer of glycosaminoglycans [81-85] and possibly damage the membrane below. In the LB experiments of this study, it is suggested that when domains of lipids are compressed, boundary defects are sometimes created where domains come together and that these linear defect sites preferentially nucleate crystal growth and result in lines of COM crystals as seen in Figure 4-7. In this way, the boundary defects of the lipid monolayer may be comparable to damaged areas of a kidney.

Figure 4-6 Brewster angle micrograph of COM crystals formed at a glycerol lipid monolayer after 90 minutes. Image dimensions are approximately 2mm x 2 mm.
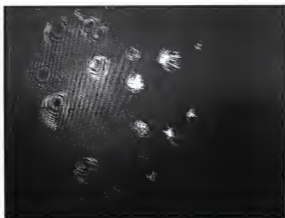
Figure 4-7   Brewster angle micrograph of a linear arrangement of COM crystals formed at a glycerol lipid monolayer. Boundary defects in lipid domains may be responsible for preferential crystal formation.

Transmission Electron Diffraction

The electron diffraction pattern in Figure 4-8 was obtained from a glycerol monolayer that was allowed to sit on a supersaturated COM subphase for 30 minutes. The aim of the experiment was to determine which crystal face of COM nucleates at the monolayer in the early stages of crystal formation. The bright diffraction spots in Figure 4-8 are from a sodium chloride crystal. Sodium chloride was commonly seen in microscopy experiments, as the subphase solution was 0.15 M NaCl. These crystals of NaCl seen in TEM and SEM experiments were not formed at the same time nor by the same mechanism as COM crystals. NaCl crystals resulted from the sample collection process, when small amounts of residual subphase solution dried on the substrate.

The diffraction rings were indexed and attributed to the {121}, {130}, {231} and {$\overline{3}$23} diffraction planes of calcium oxalate monohydrate. [86,87] In order for these planes to give diffraction rings, the COM nuclei and small crystals in the sample were oriented with their (10$\overline{1}$) faces parallel to the monolayer plane. This finding is in agreement with mature COM crystal orientations under lipid monolayers, as seen using scanning electron microscopy. The significance of the (10$\overline{1}$) face nucleating preferentially at the monolayer will be discussed in the following section.
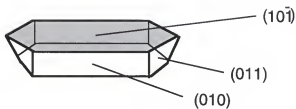
Figure 4-8. Electron diffraction pattern of COM crystals (rings) allowed to nucleate under glycerol monolayer for 30 minutes. Rings from the innermost outward correspond to the {121}, {130}, {231}, and {323} diffraction planes of COM. A sodium chloride crystal gave rise to the observed spot pattern.
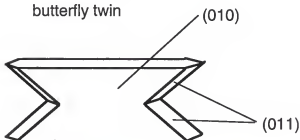
Scanning Electron Microscopy

Figure 4-9 shows two common morphologies of COM and labels their crystal faces. The shaded face ($10\bar{1}$) is the one which most commonly nucleated at the lipid monolayer. COM crystals made in bulk solution, by mixing aqueous solutions of calcium chloride and sodium oxalate together in a beaker, were predominantly of the "butterfly" twin morphology as seen in the scanning electron micrograph of Figure 4-10. However, when COM was formed under lipid monolayers, the crystals were most commonly like the one shown in Figure 4-11. This crystal was grown under a glycerol monolayer for 21 hr. The ($10\bar{1}$) face, facing upward toward the viewer, was the face that nucleated at the lipid monolayer. Nearly 100% of COM crystals with this morphology were nucleated at the (101) face, which is calcium-rich [87,88] and has a slight positive charge surplus. The lipid head groups form a negatively charged surface for nucleation, and form a Ca-rich crystal face. For these reasons it is believed thatelectrostatics are important in the formation of COM at lipid monolayers. It is worth mentioning that the (011) face of COM is also calcium-rich, and is therefore a candidate for nucleating at the lipid monolayer. This was not observed experimentally. The (011) crystal face cannot face up in SEM samples due to the crystal's geometry (see Figure 4-9). However, perhaps COM was forming from its (011) face and then falling over during sample collection. If this were the case, the crystals would fall over during sample collection to give either the ($10\bar{1}$) or the (010) face up, with nearly equal probability. An equal distribution between these two faces was not observed

COM crystal

— (10$\bar{1}$)

— (011)

(010)

butterfly twin

(010)

(011)

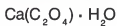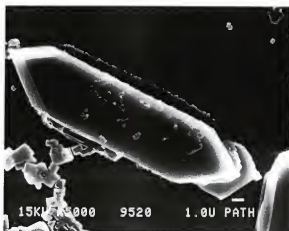**Calcium Oxalate Monohydrate (COM)**

$$Ca(C_2O_4) \cdot H_2O$$

Figure 4-9. Common morphologies of COM.

Figure 4-10. Scanning electron micrograph of COM butterfly twins formed in bulk solution. (Magnification = 2k)

Figure 4-11. Scanning electron micrograph of COM crystal nucleated at the ($10\bar{1}$) face. NaCl crystals present in lower left corner. (Magnification = 5k)

experimentally. Therefore, the (011) face is not believed to be involved in the nucleation process.

Figures 4-12 and 4-13 give examples of agglomerate COM crystals formed under arachidic acid ($C_{19}H_{39}COOH$) and serine monolayers, respectively, after 4 hrs. Attached to the bottom of the serine aggregate is NaCl. Agglomerates such as these are the result of rapid crystal growth,[83] where COM is nucleating upon itself rather than at other sites under the monolayer.

A SEM micrograph showing an area with a high density of COM crystals is shown in Figure 4-14. This sample was from a choline monolayer after 4 hr of crystal growth. The majority of crystals are oriented with the (10$\overline{1}$) face up, which nucleated at the monolayer. Indicated by arrows near the center of the micrograph is a rare occurrence of two COM crystals that nucleated at the (010) face.

It needs to be stated that when observing SEM samples where crystals were formed at monolayers, the observation of crystals was the exception rather than the rule. An average of less than ten crystals per square millimeter were found for all lipid monolayers and a typical 60 x 100 mm viewing area on the SEM would show no crystals.

It was desired to quantify the effect that the lipid head group had upon the amount of COM being produced. In doing this it was of course necessary to hold all variables constant while varying the head group. Initially, we attempted to monitor calcium consumption from the subphase as COM was produced to

Figure 4-12. Scanning electron micrograph of COM aggregates formed underneath an arachidic acid monolayer. (Magnification = 3k)

Figure 4-13. Scanning electron micrograph of a COM aggregate formed underneath a serine monolayer. (Magnification = 3.6k)
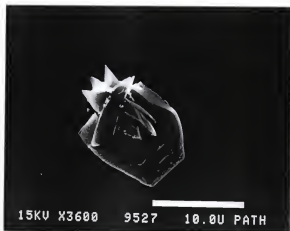
15KU X3000 - 9545   10.0U PATH

15KU X3600   9527   10.0U PATH

Figure 4-14. Scanning electron micrograph of COM formed underneath a choline monolayer. (Magnification = 0.5k)

5KV X500   9545 · 10 0U PATH

compare the lipid's COM growing abilities. However, neither the calcium ion selective electrode, atomic absorption, nor ion chromatography were able to detect the slight change in subphase calcium concentration as crystals were being formed. We estimate that the calcium concentration would drop by only 5 x 10^{-9} M during COM formation in our LB experiment, assuming 20 COM crystals form per square millimeter from 600 mL of a 5 mM Ca^{2+} subphase. Restated, the calcium concentration is expected to drop by 0.0001%. This very slight concentration change made it necessary to abandon calcium consumption measurements and attempt quantification by SEM, counting COM crystals grown per unit area.

Figure 4-15 is a bar graph showing the number of COM crystals grown per square millimeter under glycerol, serine, and choline monolayers at a subphase supersaturation level of 10 (RS = 10). For each lipid, the value shown is the average of at least 100 mm^2 of monolayer, analyzed from 2-3 separate experiments. The error bars shown represent standard deviation between samples. In general, it appears that the glycerol head group produced more COM crystals than did serine or choline. However, little more can be said since the standard deviations were so large that they obscure differences between head groups. It is believed that at the relative supersaturation level of 10 used here, too many calcium and oxalate ions are in solution to be able to discern subtle differences in the chemical nature of the monolayer. At such high supersaturation levels, the system is far from equilibrium and highly stressed. The system will precipitate rapidly upon the monolayer regardless of its chemical composition in order to lower its energy and move toward equilibrium. For this reason the study was also carried out at a lower supersaturation level. However, it is of interest to note that in some kidney stone forming patients, COM supersaturation levels in the urine can be as high as 20.[89]
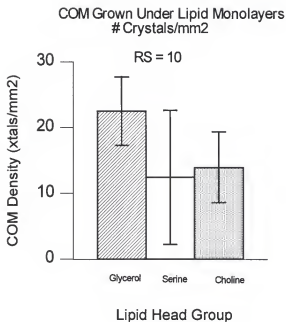
Figure 4-15. Number of COM crystals grown per square millimeter under lipid monolayers at a relative supersaturation (RS) level of 10.

The effects of changing the relative supersaturation level of COM in the subphase can be seen by observing the distribution of COM crystal morphologies. Figure 4-16 shows the distribution of crystal types grown under choline monolayers at relative supersaturation levels of 10 and 5. At an RS of 10, agglomerates constitute 25% of the crystal population. These large, polycrystalline structures are the result of rapid, uncontrolled crystal growth. When the RS level was reduced to 5, agglomerates made up only 1% of the total. The reduction in the amount of agglomerates formed at lower supersaturation levels points toward a slower, more controlled nucleation of COM.

Conducted at a lower supersaturation level of 5, Figure 4-17 shows that definite differences do exist between lipid head groups in their ability to nucleate COM. Lowering the RS level to 5 made for a slower, more controlled crystallization that allowed the chemical nature of the lipid head groups to have a more clear effect. Glycerol monolayers had nearly twice as many crystals as serine per unit area, and serine monolayers, in turn, had slightly more COM crystals than choline monolayers. The ranges of values (average value $\pm$ standard deviation) for the number of COM crystals grown per unit area given in Figure 4-17 for the diferent lipids do not overlap up to a 99% confidence level as determened by the Student's t-test. The crystal growing abilities of the lipids studied (glycerol > serine > choline) also corresponds to the anionic character of the head group. The most crystals were grown at the head group with the highest density of negative charge: glycerol. This negative charge comes from its hydroxy groups and also from the fact that it has no positively charged component to dilute the charge. Growing far fewer crystals was the zwitterionic serine head group, having both carboxylate and protonated amine groups, and

**COM Distribution
Choline**

RS = 10   RS = 5

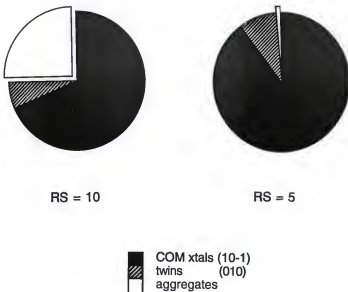COM xtals (10-1)
twins   (010)
aggregates

Figure 4-16. Distribution of COM crystal types grown under choline
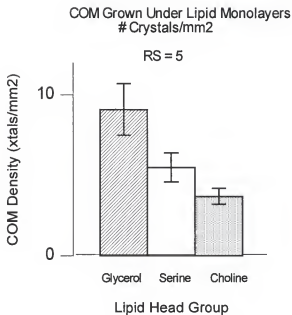monolayers at relative supersaturation (RS) levels of 10
and 5.

Figure 4-17. Number of COM crystals grown per square millimeter under lipid monolayers at a relative supersaturation (RS) level of 5.

producing the smallest number of COM crystals was the choline with its quaternary amine group.

From the trends in the number of COM crystals formed at lipid head groups, anionic > zwitterionic > cationic head groups, and the fact that the face which predominantly nucleates at the monolayer is calcium-rich, it is clear that at lower supersaturation levels, electrostatics play a large role in the nucleation of COM at lipid monolayers. The mechanism for the nucleation of COM at lipid monolayers appears to be similar to that proposed by Heywood *et al.*[23] on work with calcium carbonate forming under surfactant monolayers. A negatively charged monolayer attracts a layer of Ca^{2+} counter ions (e.g. Stern layer) from solution that mimics the calcium positions of a particular crystal face. This crystal face then serves as the nucleation site from which successive layers of the crystal grow.

We have shown that crystal growth can be controlled by the choice of the lipid monolayer. What is not yet known is whether these lipids encourage or discourage crystal growth (precipitation), relative to a more disordered surface. For example, crystal growth appears to be enhanced at what are believed to be defect areas of the monolayer, as given by lines of crystals seen in the BAM experiment. Also, when COM was formed under a polymeric monolayer of polyoctadecylmethacrylate, the crystal density was higher than for that found under lipid monolayers. This was surprising since the polymer presents a nucleation surface that is less negatively charged and less organized than that of the lipid monolayers. However, the polymer monolayer is believed to possess a rougher surface with more topographical features where crystal formation may be favored. With these observations in mind, it may be the case that a smooth, well-ordered, two-dimensional array of lipid head groups may not promote the formation of calcium oxalate monohydrate relative to a more disordered surface.

Conclusion

This study suggests that Langmuir monolayer films of lipids can be effectively used as a model for the formation of kidney stones at interfaces. This model system may mimic the process by which kidney stones are formed in the body. It was found that the number of COM crystals grown under the monolayer was related to the degree of negative charge on the lipid head group, where nucleation occurs. Head groups with more negative charge, such as glycerol, produce more COM crystals per unit area than do lipids with more cationic character. It was also found that a calcium-rich face, the $(10\bar{1})$, nucleated predominantly at the monolayer. From these findings it appears that the nucleation of COM at lipid monolayers depends heavily upon electrostatic forces.

In future studies, the LB model can be modified to resemble more closely the conditions within the kidney, for example, by using mixed lipid monolayers. One potential benefit of the model is that crystal growth inhibitors[58,90-92] may be investigated in less time than is required for traditional *in vivo* studies.

CHAPTER 5

CONCLUSIONS, PERSPECTIVE AND FUTURE WORK

The polymeric diynoic acid template of Chapter 2 was able to effectively guide the formation of large, singly oriented cadmium iodide crystals over areas 2.6 µm in diameter. However, the polymer template did not appear to limit diffusion between inorganic layers significantly better than did the monomer arachidic acid template. This inability to limit diffusion was attributed to the weaker van der Waals forces of the diynoic acid template molecules before polymerization compared to the arachidic acid molecules. The two short C_{10} and C_8 alkyl chains of the diynoic acid molecule do not have as strong of intermolecular forces as does the one long C_{19} chain of arachidic acid. Weaker van der Waals forces allow for many smaller diynoic acid domains to exist compared to the arachidic acid system. If polymerization left these smaller diyne domains intact, it may result in the formation of crystals at slightly different in-plane orientations as seen in this work. In addition, defect sites between domains could provide avenues for metal ions to diffuse between layers, forming bulk cadmium iodide particles rather than the desired cadmium iodide monolayers.

In working with Langmuir-Blodgett films of cadmium octadecylxanthate, it was found that the well ordered system could be used to form CdI_2 crystals with their 001 faces oriented exclusively parallel to the LB layer planes. This aspect

as similar to results obtained using arachidic acid films. Within the layer plane, however, crystals in the xanthate template do not have similar orientations. This was in contrast to the control arachadic and diynoic acid films have over in-plane crystal orientation of cadmium halides. The reason for the xanthate template's lack of control over in-plane orientation is that the xanthate gave off its CS_2 head group during the reaction with HI gas. Once this occurred, the organic film lost its ability to control the in-plane orientation of the particle as seen in electron diffracton data.

The effect that a LB film can have upon the formation of inorganic particles can be seen by comparing particle orientations where the organic template is intact (diynoic system) to those where part of the template is removed (xanthate system). The LB film and the head groups in particular are clearly responsible for controlling the orientation of the forming particle.

Future work on the formation of particles within bilayers of transferred LB films will focus on forming the particles in a slower, more controlled manner. In this way, the template may be able to have a more pronounced effect on the forming particles. For example, the particle-forming reaction could be slowed down by using much less HX gas (mL instead of mL). The reaction could also be carried out under a high pressure of argon rather than under vacuum. This would slow the diffusion of HX molecules to reactive sites.

The findings of Chapter 4 suggest that monolayers of lipids can be used as a model for the formation of kidney stones at interfaces. This model system may mimic the process by which kidney stones are formed in the body. It was found that the number of COM crystals grown under the monolayer was related to the degree of negative charge on the lipid head group, where nucleation occurs. Head groups with more negative charge, such as glycerol, produce more COM crystals per unit area than do lipids with more cationic character. It

was also found that a calcium-rich face, the (10$\bar{1}$), nucleated predominantly at the monolayer. From these findings it appears that the nucleation of COM at lipid monolayers depends heavily upon electrostatic forces.

In future studies, the LB model can be modified to resemble more closely the conditions within the kidney, for example, by using mixed lipid monolayers. One potential benefit of the model is that crystal growth inhibitors may be investigated in less time than is required for traditional *in vivo* studies.

LIST OF REFERENCES

(1)   Pike, J. K. Ph. D. Dissertation, University of Florida, 1994.

(2)   Pike, J. K.; Byrd, H.; Morrone, A. A.; Talham, D. R. *Chem. Mater.* 1994, *6*, 1757-1765.

(3)   Pike, J. K.; Byrd, H.; Morrone, A. A.; Talham, D. R. *J. Am. Chem. Soc.* 1993, *115*, 8497-8498.

(4)   Lowenstam, H., A.; Weiner, S. *On Biomineralization;* 1st ed.; Oxford University Press: New York, 1989, pp 324.

(5)   Heuer, A. H.; Fink, D. J.; Laraia, V. J.; Arias, J. L.; Calvert, P. D.; Kendall, K.; Messing, G. L.; Blackwell, J.; Rieke, P. C.; Thompson, D. H.; Wheeler, A. P.; Veis, A.; Caplan, A. I. *Science* 1992, *255*, 1098-1105.

(6)   Bianconi, P. A. *Biomimetic Mineralization;* 1st ed.; American Chemical Society: New York, 1995; Vol. 245, pp 522.

(7)   Mann, S. *Nature* 1988, *332*, 119-124.

(8)   Mann, S.; Heywood, B. R. *Chem. Br.* 1989, 98-101.

(9)   Addadi, L.; Moradian, J.; Shay, E.; Maroudas, N. G.; Weiner, S. *Proc. Natl. Acad. Sci. USA* 1987, *84*, 2732-2736.

(10) Mann, S.; Heywood, B. R.; Didymus, J. M.; Rajam, S.; Wade, V. J.; Walker, J. B. A. *Mat. Res. Soc. Symp. Proc.* 1990, *174*, 25-36.

(11) Mann, S. *Struct. Bond. (Berlin)* 1983, *54*, 125-180.

(12) Heywood, B. R. *Microscopy Research and Technique* 1994, *27*, 376-388.

(13) Mann, S.; Hannington, J. P.; Williams, R. J. P. *Nature* 1986, *324*, 565-567.

(14) Heywood, B. R.; Fendler, J. H.; Mann, S. J. *Colloid Interface Sci.* 1990, *1* *38*, 295-298.

(15) Meldrum, F. C.; Wade, V. J.; Nimmo, D. L.; Heywood, B. R.; Mann, S. *Nature* 1991, *349*, 684-687.

(16) Landau, E. M.; Levanon, M.; Leiserowitz, L.; Lahav, M.; Sagiv, J. *Nature* 1985, *318*, 353-356.

(17) Landau, E. M.; Popovitz-Biro, R.; Levanon, M.; Leiserowitz, L.; Lahav, M.; Sagiv, J. *Mol. Cryst. Liq. Cryst.* 1986, *134*, 323-335.

(18) Landau, E. M.; Grayer Wolf, S.; Levanon, M.; Leiserowitz, L.; Lahav, M.; Sagiv, J. *J. Am. Chem. Soc.* **1989**, *111*, 1436-1445.

(19) Mann, S.; Heywood, B. R.; Rajam, S.; Birchall, J. D. *Nature* **1988**, *334*, 692-695.

(20) Mann, S.; Heywood, B. R.; Rajam, S.; Birchall, J. D. *Proceedings of the Royal Society of London* **1989**, *A 423*, 457-471.

(21) Mann, S.; Heywood, B. R.; Rajam, S.; Walker, J. B. A. *Journal of Physics D: Applied Physics* **1991**, *24*, 154-164.

(22) Heywood, B. R.; Rajam, S.; Mann, S. *J. Chem. Soc. Faraday Trans.* **1991**, *87*, 735-743.

(23) Heywood, B. R.; Mann, S. *Chem. Mater.* **1994**, *6*, 311-318.

(24) Heywood, B. R.; Mann, S. *Adv. Mater.* **1994**, *6*, 9-20.

(25) Heywood, B. R.; Mann, S. *J. Am. Chem. Soc.* **1992**, *114*, 4681-4686.

(26) Heywood, B. R.; Mann, S. *Langmuir* **1992**, *8*, 1492-1498.

(27) Zhao, X. K.; Yang, J.; McCormick, L. D.; Fendler, J. H. *J. Phys. Chem.* **1992**, *96*, 9933-9939.

(28) Pike, J. K.; Byrd, H.; Morrone, A. A.; Talham, D. R. *Thin Solid Films* **1994**, *243*, 510-514.

(29) Tieke, B.; Lieser, G.; Wegner, G. *Journal of Polymer Science: Polymer Chemistry Edition* **1979**, *17*, 1631-1644.

(30) Tieke, B.; Graf, H.-J.; Wegner, G.; Naegele, B.; Ringsdorf, H.; Banerjie, A.; Day, D.; Lando, J. B. *Coll. Poly. Sci.* **1977**, *255*, 521-531.

(31) Ogawa, K. *Jpn. J. Appl. Phys.* **1988**, *27*, 855-860.

(32) Ogawa, K.; Tamura, H.; Hatada, M.; Ishihara, T. *Langmuir* **1988**, *4*, 195-200.

(33) Sudiwala, R. V.; Cheng, C.; Wilson, E. G.; Batchelder, D. N. *Thin Solid Films* **1992**, *210/211*, 452-454.

(34) Okada, S.; Matsuda, H.; Nakanishi, H.; Kato, M.; Otsuka, M. *Thin Solid Films* **1989**, *179*, 423-427.

(35) Kaneko, F.; Dresselhaus, M. S.; Rubner, M. F.; Shibata, M.; Kobayashi, S. *Thin Solid Films* **1988**, *160*, 327-332.

(36) Tieke, B.; Wegner, G.; Naegele, D.; Ringsdorf, H. *Angew. Chem. Int. Ed. Engl.* **1976**, *15*, 764-765.

(37) Deckert, A. A.; Horne, J. C.; Valentine, B.; Kiernan, L.; Fallon, L. *Langmuir* **1995**, *11*, 643-649.

(38) Fukuda, K.; Shibasaki, Y.; Nakahara, H. *Thin Solid Films* **1988**, *160*, 43-52.

(39) Fukuda, K.; Shibasaki, Y.; Nakahara, H.; Endo, H. *Thin Solid Films* **1989**, *179*, 103-107.

(40) Shibata, M.; Kaneko, F.; Aketagawa, M.; Kobayashi, S. *Thin Solid Films* **1989**, *179*, 433-437.

(41) Kaneko, F.; Shibata, M.; Kobayashi, S. *Thin Solid Films* **1992**, *210/211*, 548-550.

(42) Tieke, B.; Lieser, G. *J. Colloid Interface Sci.* **1982**, *88*, 471-486.

(43) Tieke, B.; Weiss, K. *J. Colloid Interface Sci.* **1984**, *101*, 129-148.

(44) Scoberg, D. J.; Grieser, F.; Furlong, D. N. *J. Chem. Soc., Chem. Commun.* **1991**, *7*, 515-517.

(45) Kern, W. *J. Electrochem. Soc.* **1990**, *137*, 1887-1892.

(46) Netzer, L.; Sagiv, J. *J. Am. Chem. Soc.* **1983**, *105*, 674-676.

(47) Liedberg, B.; Bertilsson, L. *Langmuir* **1993**, *9*, 141-149.

(48) *Practical Surface Analysis*; 2nd ed.; Briggs, D.; Seah, M. P., Ed.; John Wiley and Sons: Chichester, 1990; Vol. 1.

(49) Cotton, F. A.; Wilkinson, G. *Advanced Inorganic Chemistry*; 5th ed.; John Wiley & Sons: New York, 1988, pp 1455.

(50) Arndt, T.; Schupp, H.; Schrepp, W. *Thin Solid Films* **1989**, *178*, 319-326.

(51) Chollet, P.-A. *J. Phys. C: Solid State Phys.* **1974**, *7*, 4127-4134.

(52) Budach, W.; Ahuja, R. C.; Mobius, D.; Schrepp, W. *Thin Solid Films* **1992**, *210/211*, 434-436.

(53) Ihs, A.; Uvdal, K.; Liedberg, B. *Langmuir* **1993**, *9*, 733-739.

(54) Klein, E.; Bosarge, J. K.; Norman, I. *J. Am. Chem. Soc.* **1960**, *64*, 1666-1670.

(55) Aspila, K. I.; Joris, S. J.; Chakrabarti, C. L. *J. Phys. Chem.* **1970**, *74*, 3625-3629.

(56) Edington, J. W. *Practical Electron Microscopy in Materials Science*; Van Nostrand Reinhold: New York, 1976, pp 100.

(57) Gill, W. B. *American Journal of Kidney Disease* **1981**, *1*, 66.

(58) Smesko, A.; Singh, R. P.; Lanzalaco, A. C.; Nancollas, G. H. *Colloids and Surfaces* **1988**, *30*, 361-371.

(59) Prien, E. L.; Prien, E. L. *American Journal of Medicine* **1968**, *45*, 654.

(60) DeLong, J. D.; Briedis, D. *Journal of Crystal Growth* **1985**, *71*, 689-698.

(61) *Langmuir-Blodgett Films*; Roberts, G. G., Ed.; Plenum Press: New York, 1990.

(62) Byrd, H.; Whipps, S.; Pike, J. K.; Ma, J.; Nagler, S. E.; Talham, D. R. *J. Am. Chem. Soc.* **1994**, *116*, 295-301.

(63) Byrd, H.; Pike, J. K.; Talham, D. R. *Chem. Mater.* **1993**, *5*, 709-715.

(64) Byrd, H.; Pike, J. K.; Showalter, M. L.; Whipps, S.; Talham, D. R. In *Interfacial Design and Chemical Sensing*; T. E. Mallouk and D. J. Harrison, Ed.; American Chemical Society: Washington, 1994; Vol. ACS Symposium Series 561; pp 49-59.

(65) Byrd, H.; Whipps, S.; Pike, J. K.; Talham, D. R. *Thin Solid Films* **1994**, *244*, 768-771.

(66) Lehninger, A. L. *Biochemistry*; 2nd ed.; Worth Publishers, Inc.: New York, 1976, pp 1104.

(67) Mingotaud, A.-F.; Mingotaud, C.; Patterson, L. K. *Handbook of Monolayers*; 1st ed.; Academic Press: London, 1993; Vol. 1, pp 1378.

(68) Dhathathreyan, A.; Mobius, D. *Colloids and Surfaces* **1988**, *33*, 43-53.

(69) Seelig, J. *Cell Biology International Reports* **1990**, *14*, 353-360.

(70) Ververgaert, P. H. J. T.; De Kruyff, B.; Verkleij, A. J.; Tocanne, J. F.; Van Deenen, L. L. M. *Chemistry and Physics of Lipids* **1975**, *14*, 97-101.

(71) El Mashak, E. M.; Lakhdar-Ghazal, F.; Tocanne, J. F. *Biochimica et Biophysica Acta* **1982**, *688*, 465-474.

(72) Zidovetzki, R.; Atiya, A. W.; De Boeck, H. *Membrane Biochemistry* **1989**, *8*, 177-186.

(73) Verkleij, A. J.; De Kruyff, B.; Ververgaert, P. H. J. T.; Tocanne, J. F.; Van Deemen, L. L. M. *Biochimica et Biophysica Acta* **1974**, *339*, 432-437.

(74) Ohnishi, S.-I.; Ito, T. *Biochemistry* **1974**, *13*, 881-887.

(75) Lara-Ochoa, F. *Biophysical Chemistry* **1991**, *40*, 207-215.

(76) Okamura, E.; Umemura, J.; Takenaka, T. *Biochimica et Biophysica Acta* **1985**, *812*, 139-146.

(77) Hunt, R. D.; Mitchell, M. L.; Dluhy, R. A. *Journal of Molecular Structure* **1989**, *214*, 93-109.

(78) White, R. L.; Ai, J. *Applied Spectroscopy* **1992**, *46*, 93-99.

(79) Shippey, T. A. *Journal of Molecular Structure* **1980**, *63*, 157-166.

(80) Losche, M.; Rabe, J.; Fischer, A.; Rucha, B. U.; Knoll, W.; Mohwald, H. *Thin Solid Films* **1984**, *117*, 269-280.

(81) Khan, S. R.; Cockrell, C. A.; Finlayson, B.; Hackett, R. L. *Journal of Urology* **1984**, *132*, 153-157.

(82) Mandel, N. *Journal of the American Society of Nephrology* **1994**, *5*, S37-S45.

(83) Sohnel, O.; Grases, F. *Advances in Colloid Interface Science* **1995**, *59*, 1-17.

(84) Gill, W. B.; Ruggiero, K.; Strauss, F. H. *Invest. Urology* **1979**, *17*, 257-261.

(85) Gill, W. B.; Jones, K. W.; Ruggiero, K. J. *Journal of Urology* **1982**, *127*, 152-154.

(86) Lecomte; Pobequin; Wyart *Journal of Physics Radium* **1945**, *6*, 22.

(87) Deganello, S. *Acta Cryst.* **1980**, *B37*, 826-829.

(88) Cho, S. B. "Morphological Forms of Calcium Oxalate Monohydrate," University of Florida, 1995.

(89) Robertson, W. G.; Saw, D. S.; Bridge, D. M. *Journal of Crystal Growth* **1981**, *53*, 182.

(90) Deganallo, S. *Calcified Tissue International* **1991**, *48*, 421-428.

(91)   Asplin, J.; Deganello, S.; Nakagawa, Y. N.; Coe, F. C. *American Journal of Physiology* **1991**, *27*, F824-F830.

(92)   Singh, R. P.; Gaur, S. S.; White, D. J.; Nancollas, G. H. *J. Colloid Interface Sci.* **1987**, *118*, 379-386.

BIOGRAPHICAL SKETCH

Scott Whipps was born in Spokane, Washington on May 8, 1968 to Richard and Cathleen Whipps. He graduated from North Central High School in 1986 with a strong interest in science before attending Pacific Lutheran University in Tacoma, Washington. Here Scott played intercollegiate tennis for four years and received a Bachelor of Science in Chemistry in 1991.

After travelling aimlessly through Europe for several months, he came to the University of Florida in Gainesville to work toward a Ph.D. in Chemistry under the supervision of Dr. Daniel R. Talham. Upon completing his doctorate, Scott plans either to pursue a career of industrial research with Arizona Chemical in Panama City, Florida, or to shave his head and play drums in a punk rock band.

I certify that I have read this study and that in my opinion it conforms to acceptable standards of scholarly presentation and is fully adequate, in scope and quality, as a dissertation for the degree of Doctor of Philosophy.
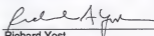
Daniel R. Talham, Chairman
Associate Professor of Chemistry

I certify that I have read this study and that in my opinion it conforms to acceptable standards of scholarly presentation and is fully adequate, in scope and quality, as a dissertation for the degree of Doctor of Philosophy.
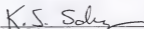
Robert Kennedy
Associate Professor of Chemistry

I certify that I have read this study and that in my opinion it conforms to acceptable standards of scholarly presentation and is fully adequate, in scope and quality, as a dissertation for the degree of Doctor of Philosophy.
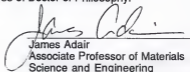
Richard Yost
Professor of Chemistry

I certify that I have read this study and that in my opinion it conforms to acceptable standards of scholarly presentation and is fully adequate, in scope and quality, as a dissertation for the degree of Doctor of Philosophy.

Kirk Schanze
Associate Professor of Chemistry

I certify that I have read this study and that in my opinion it conforms to acceptable standards of scholarly presentation and is fully adequate, in scope and quality, as a dissertation for the degree of Doctor of Philosophy.

James Adair
Associate Professor of Materials
Science and Engineering

This dissertation was submitted to the Graduate Faculty of the Department of Chemistry in the College of Liberal Arts and Sciences and to the Graduate School and was accepted as partial fulfillment of the requirements for the degree of Doctor of Philosophy.

Dean, Graduate School

December, 1996